Earliest known hominin activity in the Philippines by 709 thousand years ago

Thomas Ingicco, D. van den Bergh, C. Jago-On, J. Bahain, G. Chacón, N. Amano, H. Forestier, C. King, K. Manalo, S. Nomade, et al.

Earliest known hominin activity in the Philippines by 709 thousand years ago

T Ingicco, G D van den Bergh, C Jago-On, J-J Bahain, M G Chacón, N Amano, H Forestier, C King, K Manalo, S Nomade, et al.

Earliest known hominin activity in The Philippines by 709 thousand years ago.

T. Ingicco[1], G.D. van den Bergh[2], C. Jago-on[3], J-J Bahain[1], M. G. Chacón[4,5,1], N. Amano[6], H. Forestier[1], C. King[7], K. Manalo[7], S. Nomade[8], A. Peirera[1,8,9,10], M. Reyes[3,7], A-M. Sémah[1,11], Q. Shao[12], P. Voinchet[1], C. Falguères[1], P. Albers[13], M. Lising[7], G. Lyras[14], D. Yurnaldi[15], P. Rochette[16], A Bautista[3], J. de Vos[13]

[1] *Département Homme et Environnement, UMR 7194, Muséum national d'Histoire naturelle, Sorbonne Université, Musée de l'Homme, 17 Place du Trocadéro, 75016 Paris, France*

E-mail : ingicco@mnhn.fr

[2] *Centre for Archaeological Science, School of Earth & Environmental Sciences, University of Wollongong, Wollongong, NSW 2522, Australia*

[3] *National Museum of the Philippines, Padre Burgos St., Manila 1000, The Philippines*

[4] *IPHES – Institut Català de Paleoecologia Humana i Evolució Social, Campus Sescelades URV (Edifici W3), 43007 Tarragona, Spain*

[5] *Area de Prehistoria, Universitat Rovira i Virgili (URV), Avinguda de Catalunya 35, 43002 Tarragona, Spain*

[6] *Max Planck Institute for the Science of Human History, Kahlaische Str. 10, Jena, 07745 Germany*

[7] *Archaeological Studies Program, Albert Hall, University of the Philippines, Diliman, Quezon City 1101, The Philippines*

[8] *Laboratoire des Sciences du Climat et de l'Environnement, UMR 8212, CEA-CNRS UVSQ et Université de Paris-Saclay, 91198 Gif Sur Yvette Cedex, France*

[9] *Ecole française de Rome, Piazza Farnese 67, 00186 Roma, Italy,*

[10] *Sezione di scienze preistoriche e antropologiche, Dipartimento di Studi Umanistici, Università degli Studi di Ferrara, C.so Ercole I dle I da, C.so Ercole I de Italy*

[11] *Institut de Recherche pour le Développement, UMR LOCEAN 7159, 32 avenue Henri Varagnat, 93143 Bondy Cedex, France*

[12] *School of Geographical Sciences, Nanjing Normal University, Nanjing 210023, China*

[13] *Naturalis Biodiversity Center, P.O. Box 9517, 2300 RA Leiden, The Netherlands*

[14] *Museum of Geology and Paleontology, National and Kapodistrian University of Athens, Panepistimiopolis, 15784 Zografou, Greece*

[15] *Centre for Geological Survey, Geological Agency, Bandung 40122, Indonesia*

[16] *Aix-Marseille Université, CNRS, IRD, CEREGE UM34, 13545 Aix en Provence, France*

More than 60 years ago, stone tools and mega fauna remains were discovered on the Southeast Asian islands of Flores, Sulawesi and Luzon, and a Middle Pleistocene colonization by *Homo erectus* was initially proposed for these islands[1-4]. However, until the discovery of *Homo floresiensis* in 2003, claims for the presence of archaic hominins on Wallacean islands were hypothetical due to the absence of *in situ* fossils and/or stone artefacts excavated from well-documented stratigraphic contexts, or because secure numerical dating methods of sites were lacking. As a consequence, these claims were generally treated with scepticism[5]. Recent excavations at Kalinga in the Cagayan Valley of northern Luzon in The Philippines have yielded 57 stone-tools associated with an almost complete disarticulated skeleton of *Rhinoceros philippinensis* showing clear signs of butchery, together with other fossil fauna remains attributed to stegodon, Philippine brown deer, fresh-water turtle and monitor lizard. All finds originate from a clayey bone bed dated to between 777 thousand and 631 thousand years ago using electron-spin resonance method applied on tooth enamel and fluvial quartz. This evidence pushes back the proven period of colonization[6] of The Philippines by hundreds of thousands of years, and furthermore suggests that early overseas dispersal in Island South East Asia (ISEA) by premodern hominins took place several times during the Early and Middle Pleistocene[1-4]. The Philippines therefore may have played a central role in southward movements into Wallacea, not only of Pleistocene mega fauna[7], but also archaic hominins.

The most recent recoveries in Flores[8,9] and Sulawesi[10] (Indonesia) provide a unique documentation of over-seas hominin dispersal during the early Middle Pleistocene. An early presence in The Philippine archipelago has been speculated since the 1950s, with the reporting of presumably Pleistocene mega-faunal remains and 'Palaeolithic' industries consisting of chopping-tools and flakes (the 'Cabalwanian' and 'Liwanian' Industries respectively) from surface finds and excavations in the Cagayan Valley basin of northern Luzon[3,4]. Despite the fact that these early discoveries took place more than 60 years ago, no direct association between mega-fauna and lithic industries has ever been documented since then, and no secure numerical dating of both fossil fauna and lithics has been available

for this region[11]. To date, the discovery of a human metatarsal in Callao Cave in northern Luzon[6], directly dated at 66.7 ± 1.0 ka, represented the oldest evidence for the peopling of The Philippines.

In 2013, a survey of the Cagayan Valley near the Rizal Municipality (Kalinga Province) led to the discovery of a concentration of vertebrate bones and stone artefacts scattered on the surface near what became our new excavation site. The Kalinga site (17°33'45.0318"N; 121°33'35.7372"E) (Fig. 1,b) has been excavated annually since 2014 and has resulted in the discovery of *in situ* mega-fauna and associated stone artefacts. The substrate consists of the upper part of the Awidon Mesa Formation, a 400m thick sequence of alluvial stream deposits (mainly sandstones and claystones) intercalated with volcaniclastic and pyroclastic layers (Fig. 1a). These sediments were deposited on an alluvial fan system in braided streams of the paleo-Chico River as a consequence of uplift in the Central Cordillera to the west[12,13]. During a poorly constrained Pleistocene phase of folding in response to east-west compression, alluvial fan deposition in the Kalinga area came to a halt.

We conducted the main 16m² excavation at the head of a modern, dry stream valley, north of a small hill and down to a maximum depth of 2m (Fig. 1c, see Supplementary Information: excavation methods and Sedimentology). A 25m x 1m slot trench was excavated down the hill to the Main Excavation. Together, these excavations revealed a total of 7.5m of stratigraphy comprising four main sedimentary units, in ascending order: Unit A, Unit F, Unit G and Unit J (Fig. 1d,e; Extended Data Fig. 1). An almost complete disarticulated skeleton of *Rhinoceros philippinensis* (Extended Data Fig.2) was found embedded in the basal sediments of Unit F lying across the base of an erosional channel surface that cuts down vertically into sandy Unit A. This channel was filled with an up to 3.25m thick mudflow (Unit F; see Extended Data Fig. 3 and 4), which covered the bones, along with an *in situ* tektite as well as 57 stone-tools and sparse fossils of other animals (Geoemydidae, *Varanus* cf. *salvator*, *Stegodon* cf. *luzonensis* and *Cervus* cf. *mariannus*) (see Supplementary Information: Faunal analysis). The archaeological layer (Unit F) is conformably overlaid by a ~1.15m thick, sterile, cross-bedded coarse sandy fluvial unit with silty lenses (Unit G), which is in turn conformably overlaid by Unit H, a 2.5m thick silty pedogenised layer with rhyzoliths.

The 57 stone artefacts account for six cores, 49 flakes and two possible hammer stones, all originating from Unit F (Fig.2, see Supplementary Information: Lithic analysis). With the exception of the two possible hammer stones (Fig.2b), all artefacts lack a patinated lustre and have a fresh appearance, indicating that any transport was minimal. The knapping strategies were oriented towards short and unorganized core reduction, resulting in non-standardized flake morphologies and dimensions, and all artefacts were lacking any intentional retouch. The Kalinga lithic assemblage is diverse in its techniques, technology and final products, and appears similar to the chert industry described at Arubo 1 site[14] (See Supplementary Information: Lithic technology). Also recovered from the Unit F excavation area was a 600g pebble among hundreds of pebbles all lighter than 200g, and which we interpret as a possible manuport.

Among the more than 400 bones recovered from Unit F, the most striking remains are a disarticulated, ~75% complete skeleton of a single *Rhinoceros philippinensis* individual (Fig. 3; Extended Data Fig. 2). The bones were found lying on top of the erosional surface down-cutting Unit A, and were embedded in the basal clayey sediments of Unit F along the deepest part of the paleo-channel bed (Extended Data Fig. 3). Although none of the rhinoceros bones were found articulated, the recovered skeletal elements occur within a 3m x 2m area, suggesting that disarticulation occurred sub-aerially and that transport prior or during deposition of mudflow Unit F was minimal.

Thirteen of the excavated rhino bones, all of which in life had a thin cover of soft tissue (i.e. the ribs and metacarpals)[15,16], display cut marks (Fig. 3; Extended Data Fig. 2). Both rhinoceros humeri have similar percussion marks on the anterior surface for the right humerus and on the posterior surface for the left humerus, and both were presumably made with the intention to smash the bones and gain access to the marrow[17]. This percussion action resulted in the breakage of the left humerus into five pieces, which is the only bone found fragmented – and yet the fragments were still clustered together within a small $1m^2$ area of the excavation. On the right humerus, however, percussion did not result in fragmentation of the bone (Fig. 3).

To constrain the age of the bone-bed and the stone artefacts it contained, we applied three different dating methods to various materials (Fig. 1). Single crystal $^{40}Ar/^{39}Ar$ dating was applied to

112 plagioclase crystals from the sandy units directly below and above the archaeological Unit F and yielded
113 two statistically undistinguishable weighted mean ages of 1050 ± 28 ka and 1007 ± 29 ka, respectively
114 (1σ confidence interval) (see Supplementary Information: $^{40}Ar/^{39}Ar$ dating and Extended Data Fig. 5).
115 These $^{40}Ar/^{39}Ar$ dates yielded an age for the formation of the volcanic plagioclase crystals. Quartz grains
116 from the same two sandy units were also dated using the Electron Spin Resonance (ESR) method[18], and
117 resulted in a maximum depositional age of 727 ± 30 ka for the deposition of Unit A, and a minimum
118 depositional age of 701 ± 70 ka for Unit G (1σ confidence interval) (see Supplementary Information:
119 ESR dating).

120 To directly constrain the age of the rhinoceros skeleton and the cut-marks, we applied
121 ESR/uranium-series dating on the enamel of the rhinoceros's right maxillary third premolar from the
122 Unit F bone-bed. The tooth yielded an age of 709 ± 68 ka (1σ confidence interval), which is in agreement
123 with the ESR results on quartz (Fig. 1; see Supplementary Information: ESR-uranium series dating,
124 Extended Data Fig. 6, Extended Data Table 1 and Supplementary Information Table 1). In addition, a
125 palaeomagnetic sample was taken from a laminated silty lens in the lower part of Unit G and was found
126 to have a normal magnetic polarity (see Supplementary Information: palaeomagnetic dating and
127 Extended Data Fig. 7). The presence in Unit F of a reworked Australasian tektite (see Supplementary
128 Information: Non-destructive characterization of the tektite, Extended Data Fig. 8), which was formed
129 during a major meteoritic impact just before the onset of the Brunhes Normal polarity epoch at 781
130 ka[19,20], also provides further support for these closely grouping dating results. These results further
131 suggest that the volcanic plagioclase crystals from unit G on which the $^{40}Ar/^{39}Ar$ date was obtained were
132 reworked from older volcanoclastic deposits, and therefore provide a maximum age for the sequence
133 (see Supplementary Information: Sedimentology). Taken together with the ESR dating results, it follows
134 that the rhinoceros skeleton was buried by a mudflow at least 631 thousand years ago.

135 Our excavations at Kalinga and the numeric dating results clearly provide the first securely dated
136 evidence for human colonization of The Philippines by the early Middle Pleistocene, and long before
137 the appearance of modern humans in both the local context and wider ISEA region[21]. Although the
138 identity of these archaic toolmakers remains unknown, it is likely that they dispersed over at least one

sea barrier to reach Luzon Island[22]. The most likely points of origin are Borneo through Palawan to the west, or China through Taiwan to the north, this latter island being connected to mainland Asia during periods of low sea-level[23]. The Middle Pleistocene fauna from the Awidon Mesa Formation contains a wider range of vertebrates than the Pleistocene faunas from two islands to the south of The Philippines that have both yielded evidence for the occupation by premodern humans, Sulawesi[9] and Flores[26] (Extended Data Fig. 9). Overseas dispersal throughout Wallacea of land mammals, including hominins, could have been primarily but not exclusively in a north to south direction, following the major surface current flow patterns.

Beyond the chronological gap yet to be filled, a question clearly linked to our discovery is the origin of the Callao Cave hominin dated at 66.7 ± 1 ka. This diminutive Callao hominin may represent a direct descendent from a Pleistocene migration stock related to these early Kalinga toolmakers – similar to what happened on Flores Island – or may be derived from a more recent migration wave of anatomically modern humans[6,21,24,25].

Despite the current evidence, it still seems too farfetched to suggest that *Homo erectus*, or another as yet unknown Pleistocene ancestral candidate for the Kalinga toolmakers (e.g. 'Denisovans'[27]), were able to construct some sort of simple watercraft and deliberately cross sea barriers to reach these islands[28]. However, considering evidence of over-seas dispersal during the Middle Pleistocene is increasing in number[29,30], such a hypothesis cannot currently be rejected.

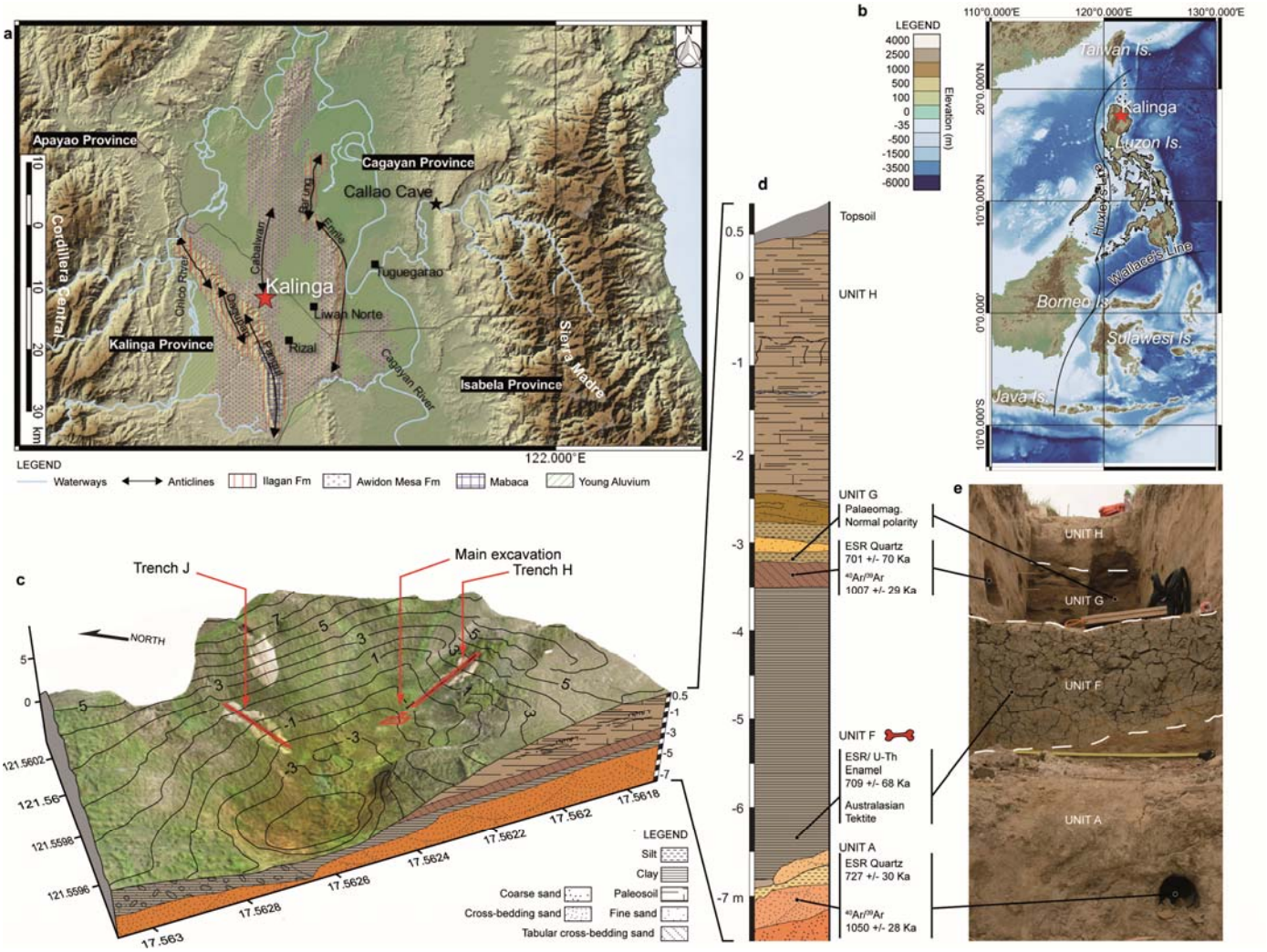

157

158 **Figure 1 | Geology and sedimentology of the Kalinga Excavation site. a**, Digital elevation map of the Cagayan Valley
159 surrounding the Rizal municipality (located in **b**, Northern Luzon Island, east of Huxley's and north of Wallace's Lines). The
160 Kalinga site (red star) is located at the southern tip of the weakly folded Cabalwan Anticline. Geological units of the area
161 bounded by the Cagayan River on the East and the Chico River on the West are after Mathisen (1981)[13]. Stratigraphically, the
162 site layers pertain to the upper part of the Awidon Mesa Formation, a Pleistocene sequence of alluvial stream deposits
163 intercalated with volcaniclastic and pyroclastic deposits. The depositional environment of the Awidon Mesa Formation was
164 characterized by braided rivers on an alluvial fan system that formed in response to uplift in the Cordillera Central to the
165 West[12,13]. **c**, Contour map of the Main Excavation and the adjoining slot Trench H along the small valley where the Kalinga site
166 is located. **d**, Detailed stratigraphy of the excavation with the absolute ages of the sedimentary units. Unit A constitutes a fining
167 upward complex of sandy to silty cross-bedded fluvial sediments. The top of Unit A is eroded and cuts down vertically over at
168 least 2.5 m. This erosive channel is filled with Unit F, a poorly sorted mudflow deposit with a maximum thickness of 3.25 m.
169 The rhino skeletal elements and most of the stone artefacts were found lying directly above the erosional contact, and were
170 found embedded in the clayey mud of Unit F. Unit F is conformably overlaid by a sequence of horizontally layered coarse
171 sandy to silty layers (Unit G), which is in turn conformably overlaid by a thick sequence of silty deposits overprinted by

paleosols (Unit H). **e**, Southward view of Trench H showing the lower and upper contacts between mudflow Unit F and sandy Unit G and between sandy Unit A and mudflow Unit F.

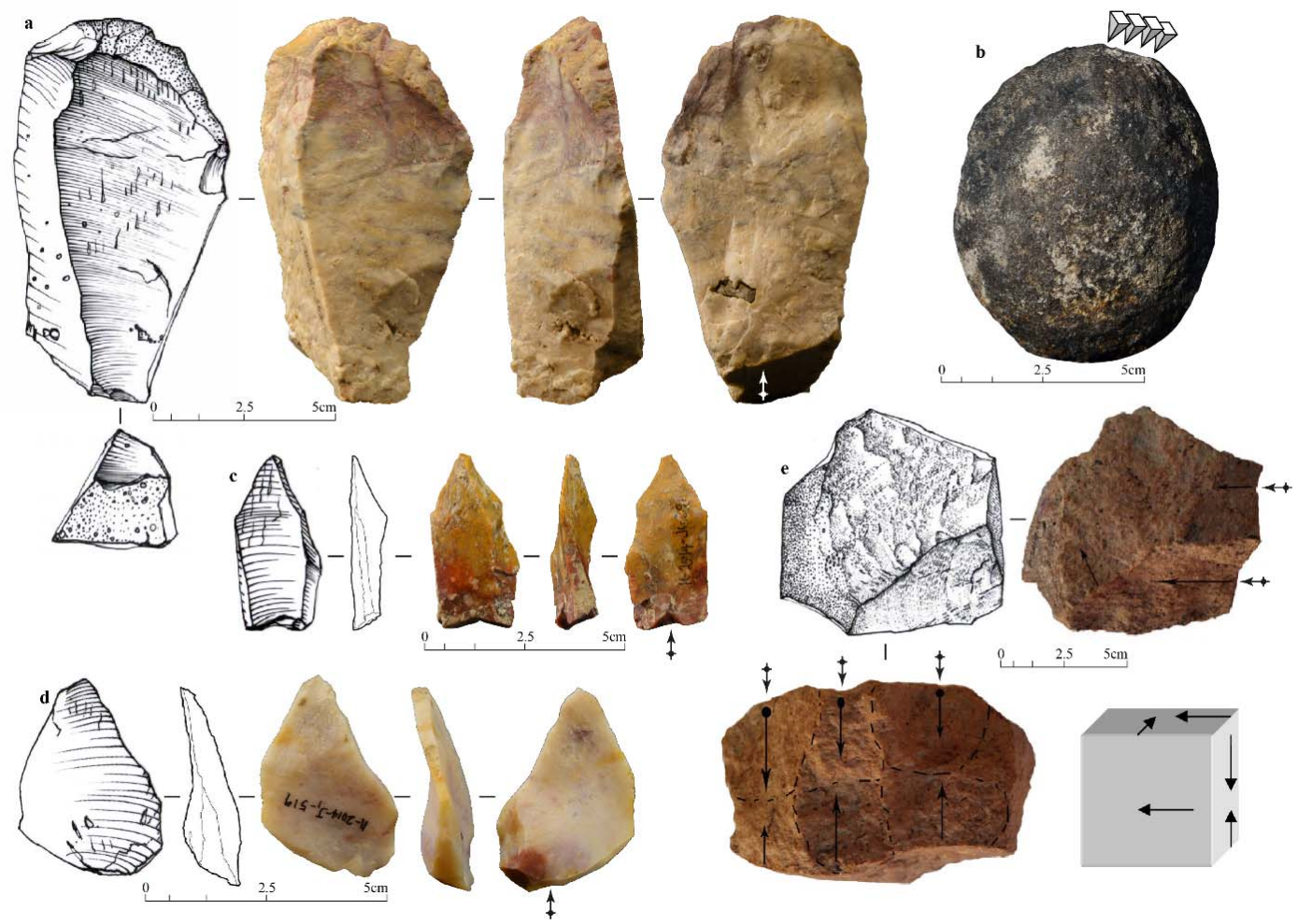

174

175 **Figure 2 | Lithic artefacts from Kalinga**. **a**, Cortical flake on chert (II-2014-J1-362; L= 100, B= 55, Th=33mm); **b**, possible
176 hammerstone on dacite (II-2014-J1-371), although its highly eroded aspect precludes any definitive conclusion; **c**, Siret
177 kombewa flake on jasper (II-2014-J1-391; L=40, B=18, Th=8mm) having a longitudinal and oblique fracture on the inferior
178 two-thirds of the left side resulting from a knapping accident while flaking; **d**, double-backed flake on flint (II-2014-J1-519);
179 **e**, core on quartz (II-2014-J1-396) -showing clear marks of knapping on anvil- with its diachritic diagram.

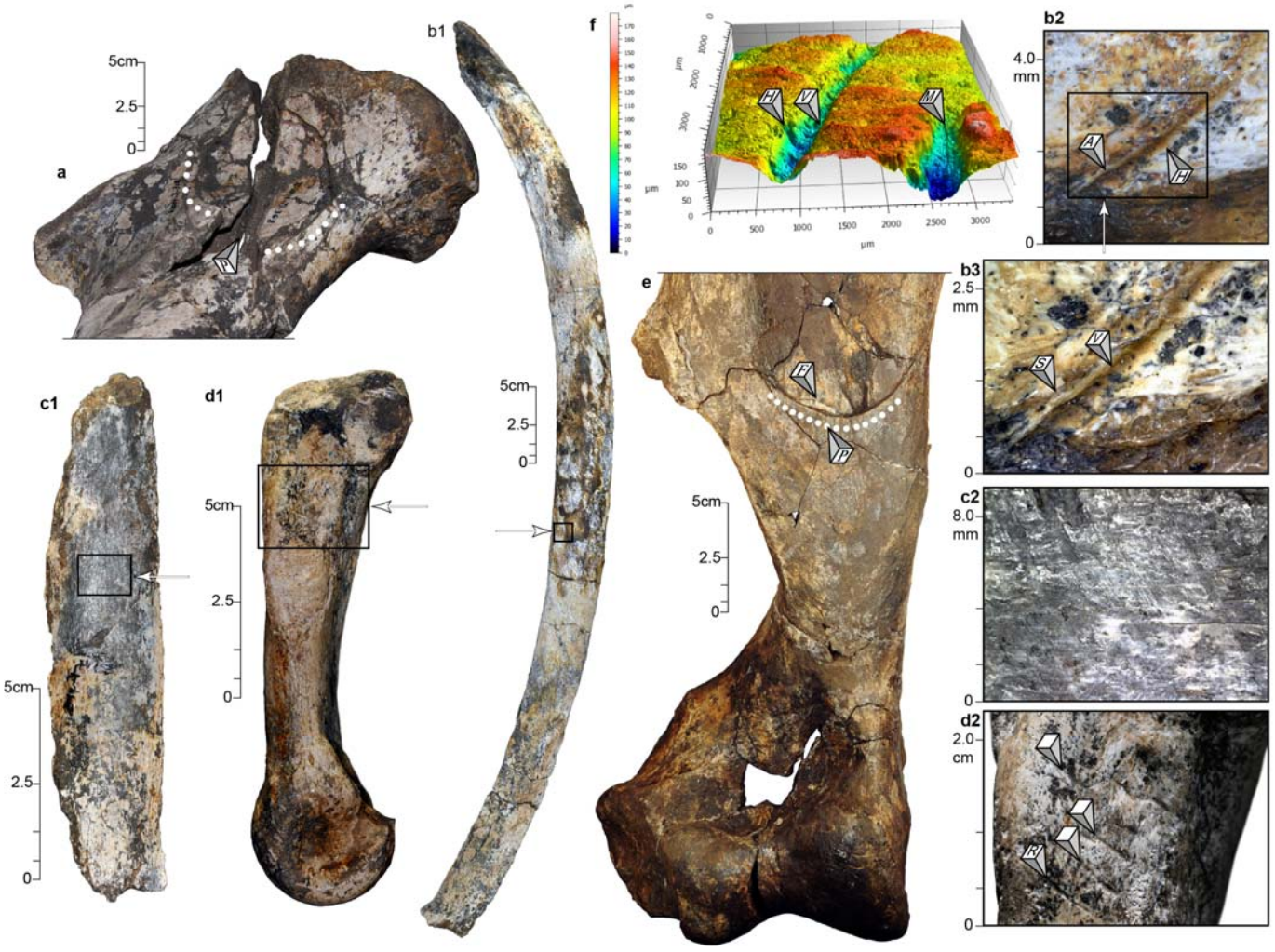

Figure 3 | Different types of marks at the surface of the bones. a, Left humerus (II-2014-J1-368) found broken into three fragments in the excavation with an anthropogenic conchoidal percussion mark (P) on its anterior surface most likely produced to get access to the marrow; **b1**, **b2** and **b3**, sub-complete rib (II-2014-J1-475), having a diagnostic anthropogenic cutmark with V-shape cross-section (V), hertzian cones (H), asymmetrical profile (A) and shoulder effect (S) on its lateral surface resulting from defleshing. Black stains are also present inside the cutmark resembling the ones observed on the surface of the rib and are the result of taphonomic processes that occurred after this cutmark was made (see Fernández-Jalvo and Andrews, 2016: 156)[17]; **c1** and **c2**, rib fragment (II-2014-J1-403) having a shiny surface on its lateral face resulting from multiple multidirectional striations, presumably due to trampling; **d1** and **d2**, right metacarpal IV (II-2014-J1-282) with parallel and rectilinear anthropogenic cutmarks (R) on its medial surface presumably generated during disarticulation; **e**, right humerus (II-2014-J1-289) with an anthropogenic conchoidal percussion mark (P) similar in size and shape to the percussion mark on the left humerus, but located on its posterior surface and more distally and associated with a small adhered bone flake (F) (see Fernández-Jalvo and Andrews, 2016: 298)[17]; **f**, three-dimensional surface topography of another rib (II-2014-J1-466) showing a linear mark (on the left) with V-shaped cross-section (V) of anthropogenic origin, as well as hertzian cones (H) and a linear mark (on the right)

with a base as broad as the heights of the walls of the grove, commonly attributed to trampling but also with assymetrical walls and possible microstriations in the bottom (M) of the groove, commonly attributed to anthropogenic marks.

References

1 van Heekeren, H. R. Early man and fossil vertebrates on the island of Celebes. *Nature* 163, 492 (1949).

2 Maringer, J. & Verhoeven, T. Die steinartefakte aus der *Stegodon*-fossilschicht von Mengeruda auf Flores, Indonesien. *Anthropos* 65, 229-247 (1970).

3 von Koenigswald, G. R. Preliminary report on a newly-discovered Stone Age culture from northern Luzon, Philippine Islands. *Asian Perspectives* 2, 69-70 (1958).

4 Fox, R. B. The Philippine Paleolithic. In *Paleolithic in South and East Asia*. 59-85 (Mouton Publishers, 1978).

5 Heaney, L.R. Zoogeographical evidence for Middle and Late Pleistocene land bridges to the Philippines islands. *Modern Quaternary Research in Southeast Asia* 9, 127-143 (1985).

6 Mijares, A. S. *et al.* New evidence for a 67,000-year-old human presence at Callao Cave, Luzon, Philippines. *Journal of Human Evolution* 59, 123-132 (2010).

7 Ingicco, T. *et al.* A new species of *Celebochoerus* (Suidae, Mammalia) from the Philippines and the paleobiogeography of the genus *Celebochoerus* Hooijer, 1948. *Geobios* 49, 285-291 (2016).

8 Brumm, A. et al. Hominins on Flores, Indonesia, by one million years ago. *Nature* 464, 748-752 (2010).

9 van den Bergh, G. D. *et al. Homo floresiensis*-like fossils from the early Middle Pleistocene of Flores. *Nature* 534, 245-248 (2016).

10 van den Bergh, G. D. *et al.* Earliest hominin occupation of Sulawesi, Indonesia. *Nature* 529, 208-211 (2016).

11 Dizon, E. Z. & Pawlik, A. F. The lower Palaeolithic record in the Philippines. *Quaternary International* 223-224, 444-450 (2010).

12 Mathisen, M. & Vondra, C. The fluvial and pyroclastic deposits of the Cagayan Basin, northern Luzon, Philippines—An example of non-marine volcaniclastic sedimentation in an interarc basin. *Sedimentology* 30, 369-392 (1983).

13 Mathisen, M. E. *Plio-Pleistocene geology of the Central Cagayan Valley, Northern Luzon, Philippines* PhD thesis, Iowa State University, (1981).

14 Pawlik, A.F. The Paleolithic site of Arubo 1 in Central Luzon, Philippines. *Indo-Pacific Prehistory Association Bulletin* 24, 1-10 (2004).

15 Yravedra *et al.* Cut marks on the Middle Pleistocene elephant carcass of Áridos 2 (Madrid, Spain). *Journal of Archaeological Science* 37, 2469-2476 (2010).

16 Mosquera *et al.* Barranc de la Boella (Catalonia, Spain): an Acheulean elephant butchering site from the European late Early Pleistocene. *Journal of Quaternary Science* 30:7, 651-666 (2015).

17 Fernandez-Jalvo, Y. & Andrews, P. *Atlas of Taphonomic Identifications* (Springer, 2016)

18 Shao, Q. *et al.* New ESR/U-series data for the early middle Pleistocene site of Isernia la Pineta, Italy. Radiation Measurements 46:847-852. (2011)

19 Lee, M.-Y., Chen, C.-H., Wei, K.-Y., Iizuka, Y. & Carey, S. First Toba supereruption revival. *Geology* 32, 61-64 (2004).

20 Valet, J-P. *et al.* Geomagnetic, Cosmogenic and Climatic changes across the last geomagnetic reversal from Equatorial Indian Ocean sediments. *Earth and Planetary Science Letters* 397:1, 67-79 (2014).

21 Liu, W. *et al.* The earliest unequivocally modern humans in southern China. Nature 526, 696-699 (2015).

22 Wang, P. & Li, Q. Oceanographical and geological background. *In* P. Wang & Q. Li (ed.), *The South China Sea: Paleoceanography and Sedimentology*, vol.13. 25-73. (Springer, 2009).

23 Voris, H.K. Maps of Pleistocene sea levels in Southeast Asia: shorelines, river systems and time durations. *Journal of Biogeography* 27, 1153-1167 (2010)

24 Détroit, F. *et al.* "Small size" in the Philippine human fossil record: Is it meaningful for a better understanding of the evolutionary history of the negritos? *Human Biology* 85:1-3, 45-66 (2013).

25 Sutikna, T. *et al.* Revised stratigraphy and chronology for *Homo floresiensis* at Liang Bua in Indonesia. *Nature* 532, 366-369 (2016).

26 Brumm, A. *et al.* Age and context of the oldest known hominin fossils from Flores. *Nature* 534, 249-253 (2016).

27 Cooper, A. & Stringer, C. Did the Denisovans Cross Wallace's Line? Science 342, 321-323 (2013).

28 Ruxon, G.D. & Wilkinson, D.M. Population trajectories versus planned colonisation of islands. *Journal of Human Evolution* 63:3, 507-511 (2012).

29 Erlandson, J.M. & Fitzpatrick, S.M. Oceans, Islands, and Coasts: Current perspectives on the role of the sea in Human Prehistory, *The Journal of Island and Coastal Archaeology* 1:1, 5-32 (2010).

30 Dennell, R.W., Louys, J., O'Regan, H.J. & Wilkinson, D.M. The origins and persistence of *Homo floresiensis* on Flores: biogeographical and ecological perspectives. *Quaternary Science Reviews* 96, 98-107 (2014).

Supplementary Information is available in the online version of the paper.

Acknowledgements Jeremy Barnes and Ana Labrador kindly provided support for this research as well as Gisela Concepcion and Marcelo dela Cruz Jr. The Kalinga excavation project was funded by the French Department for Foreign Affairs (Project MARCHE, to T.I.), The National Museum of The Philippines (to C.J-o and M.C.R.), The University of the Philippines Diliman Research Grant of the Office of Vice President for Academic Affairs (to T.I.) and the European Social Fund (Project ISOLARIO, NSRF Thalis-UOA, to G.L.). T.I. also received funding from a National Geographic Global Exploration grant (HJ-035R-17), from the French Centre National de la Recherche Scientifique (GDRi

PalBiodivASE with Valéry Zeitoun) and from Sorbonne Universités (Project MH@SU TAPHO). G.v.d.B. received funding from an Australian Research Council (ARC) Future fellowship (FT100100384). J.d.V. received funding from the Quaternary and Prehistory Erasmus Mundus Program. Additional funding was provided by the Embassy of France to The Philippines and by the Rizal Municipality. M.G.C. received funding from CERCA Programme/Generalitat de Catalunya. Authors would like to thank Susan Hayes for her feedback on the manuscript. We thank Marie-Madeleine Blanc-Valleron for providing access to the X-Ray diffractometer. A. Ledoze, S. Puaud, V. Scao, S. Baillon, H. Guillou, J. Marteau, M. Bigerelle, R. Deltombe, D. Borshneck and F. Demory are thanked for their valuable help in the laboratory analyses.

Author Contributions T.I., J.d.V. and A.B. conceived the study with C.J-o. and G.v.d.B. in collaboration with N.A., G.L. and P.A. The site stratigraphy was recorded and analysed by G.v.d.B. Samples for ESR/U-series dating were analysed by J-J.B., Q.S. and C.F. Samples for ESR dating on quartz were analysed by P.V. Samples for $^{40}Ar/^{39}Ar$ dating were analysed by S.N. and A.P. D.Y. analysed samples for palaeomagnetism. The lithic material was studied by H.F. and G.C. Palaeobotanical remains were analysed by A-M.S. and C.K. The faunal and taphonomical analysis was conducted by T.I., K.M., M.R. and N.A. T.I. and G.v.d.B. wrote the manuscript

Author Information reprints and permissions information is available at www.nature.com/reprints. The authors declare no competing financial interests. Readers are welcome to comment on the online version of the paper. Correspondence should be addressed to T.I. (ingicco@mnhn.fr). Requests for materials should be addressed to M.C.R. (mariancreyes@gmail.com).

Extended data legends

Extended Data Figure 1 | Geology and sedimentology of the Kalinga Excavation site. a, Detailed stratigraphic drawing of Trench H also showing the East wall of the S quadrant of the main Excavation. The sedimentary patterns are the same as in Figure 1. Representative logarithmic grainsize diagrams are shown for samples from each sedimentary unit; **b,** Detailed stratigraphic drawing of the Main Excavation walls; **c,** Overview towards the northwest of the quadrants N and NW of the Main Excavation in 2015. The concentration of faunal remains and stone tools lying at the base of Unit F is exposed, just above the eastward sloping erosional contact with Unit A; **d,** Detailed view of quadrant NW showing the position of a flake lying next to the rhinoceros left femur; **e,** Detail of quadrant N showing the piece of waterlogged wood fragment (yellow outline) recovered near a rhinoceros rib extremity (blue outline); **f,** Detail of quadrant NE showing the tektite recovered in Unit F along with the faunal and lithic remains.

Extended Data Figure 2 | Faunal remains from Kalinga archaeological Unit F. a, Drawing showing the preservation of the rhinoceros and position of the taphonomical marks. A total of 97 fragments of ribs of all sizes have been recovered and not all of them could be clearly positioned on the skeleton. We estimate that about 75% of the skeleton has been recovered. **b,** Fibula of *Varanus salvator*. **c,** Radius of a Cervidae. **d,** Molar of *Cervus* cf. *mariannus*. **e,** Molar fragment of *Stegodon* cf. *luzonensis*.

Extended Data Figure 3 | Digital Elevation Model (DEM) of the Main Kalinga Excavation, showing the contact surface topography between Unit A and Unit F and the vertical projections (black squares) of the archaeological materials (coloured points) on this surface. This DEM has been produced by interpolation through a kriging method from 37 three-dimensional coordinates recorded in the Main Excavation with a Total station on the erosional surface that cuts down into Unit A. This surface of contact corresponds to an erosional channel cutting down into sandy Unit A. All the material has been recovered lying across the base of the clayey Unit F along this channel, between 0.7m and 1.3m deep.

Extended Data Figure 4 | X-ray diffraction pattern of powdered Unit F clays. CPS is counts per second. Cu K-alpha corresponds to the wavelength. Quartz corresponds to the bipyramidal quartz crystals, some of which are visible to the naked eye. Bipyramidal quartz, albite, hornblende, nontronite and saponite all have a volcanic origin. Albite are plagioclase feldspar frequent in pegmatites. Hornblende is a common silicate mineral in igneous and metamorphic rocks. Nontronite is an iron-rich smectite type of clays which can be produced by hydrothermal alteration. Similarly, the smectite mineral saponite results from alteration of volcanic glass. The mineral composition of Unit F supports the interpretation as a mudflow set in a volcanic environment.

Extended Data Figure 5 | $^{40}Ar/^{39}Ar$ fusion ages of single potassium feldspar crystals for samples from Unit A and Unit G, presented as probability diagrams (**a**) that are correlated to the related inverse isochrones (**b**).

Individual ages in **a** are ± 1σ.

Extended Data Figure 6 | Measurements of dose rates (Da) and calculation of equivalent dose (De) to compute the ESR ages from quartz crystals and tooth enamel. a, Al and Ti centre ESR spectra of natural and bleached aliquots for Unit A quartz showing that Al signal is not totally reset although not measurable because extremely weak and covered by noise. **b**, ESR Dose-response curve obtained for the rhinoceros tooth (Archaeological number: II-2014-J1-095; sample code: CGY1501). The equivalent dose (DE) was extrapolated using a single saturating exponential function (Origin Microcal software) following the recommendations of Duval and Grün[9] (DE< 500 Gy, so Dmax< 5000Gy for this sample). Vertical bars account for the standard deviation around the mean for each measurement. The red curve is for the dose-response curve. The blue curves account for the 95% confidence interval of the dose-response curve. **c-f**, ESR Dose Response curves, for Aluminium (Al) and Titanium-Lithium (Ti-Li) centers of layers G1 and A4. Vertical bars account for the standard deviation around the mean for each measurement. The red curve is the dose-response curve. The blue curves account for the 95% confidence interval of the dose-response curve.

Extended Data Figure 7 | Progressive demagnetization curves (lower left of each panel), equal area projection stereoplots (upper left) and Zijderveld diagrams (right) for the six analysed specimens from Layer G_2. a-e: specimens treated by alternating field demagnetization; **f**, specimen HT-1E treated by thermal demagnetization. Open circles in the Zijderveld diagrams represent the inclination while closed circles represent declination. Open and closed circles in the equal area projection (stereoplot) represent the upper and lower hemisphere, respectively. Equal-area projections of the mean ChRMs directions of all analysed specimens, **g**, before and **h**, after demagnetization. Solid squares represent the upper hemisphere. Black cross indicates the mean ChRMs direction of the six specimens combined, surrounded by the α95circle. Red cross represents the present-day magnetic direction.

Extended Data Figure 8 | Analysis of the Kalinga tektite recovered from the archaeological layer Unit F. **a**, picture of the tektite: **b**, μXRF spectra (un-indexed peaks correspond to the Rh source) showing its composition: c, comparison of the Kalinga tektite glass composition through μXRF with an australasite tektite from China measured in the same conditions (red squares) and with an average australasite composition (blue diamonds) following Koeberl[50].

Extended Data Figure 9 | Fauna diversity of the Kalinga site as compared to contemporaneous faunas from other islands in the region. Contemporaneous to those faunas are 'classic' *Homo erectus* faunas on Java Island[97], the Mata Menge Fauna of Flores Island, which includes the putative ancestor of *Homo floresiensis*[98], and the Walanae Fauna on the southwestern branch of Sulawesi[99,100]

Extended Data Table 1 | ESR/U-series results for the rhinoceros tooth. a, U-series data for the tooth CGY1501. b, ESR/U-series data and age.

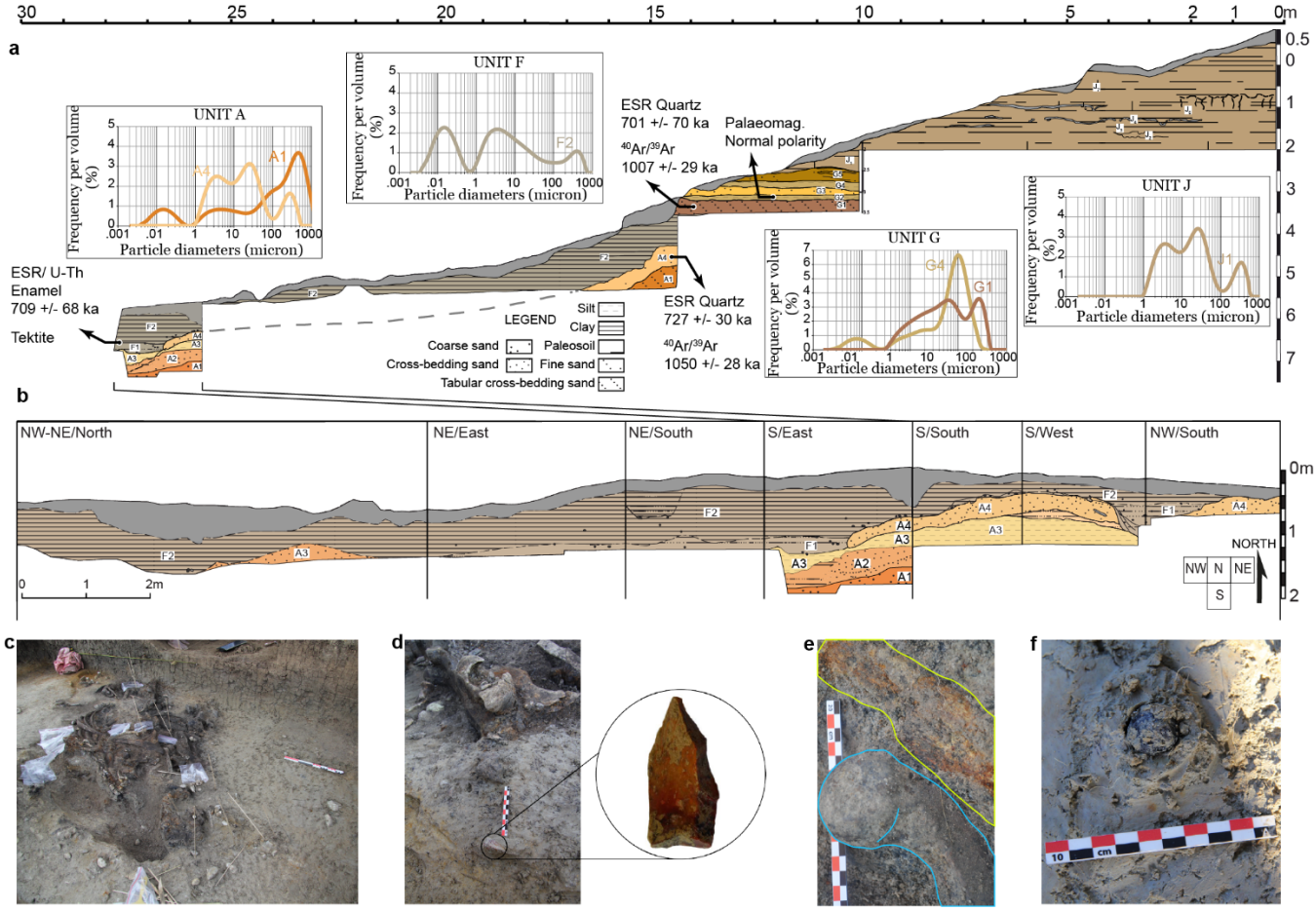

Extended Data Figure 1 | Geology and sedimentology of the Kalinga Excavation site. a, Detailed stratigraphic drawing of Trench H also showing the East wall of the S quadrant of the main Excavation. The sedimentary patterns are the same as in Figure 1. Representative logarithmic grainsize diagrams are shown for samples from each sedimentary unit; **b,** Detailed stratigraphic drawing of the Main Excavation walls; **c,** Overview towards the northwest of the quadrants N and NW of the Main Excavation in 2015. The concentration of faunal remains and stone tools lying at the base of Unit F is exposed, just above the eastward sloping erosional contact with Unit A; **d,** Detailed view of quadrant NW showing the position of a flake lying next to the rhinoceros left femur; **e,** Detail of quadrant N showing the piece of waterlogged wood fragment (yellow outline) recovered near a rhinoceros rib extremity (blue outline); **f,** Detail of quadrant NE showing the tektite recovered in Unit F along with the faunal and lithic remains.

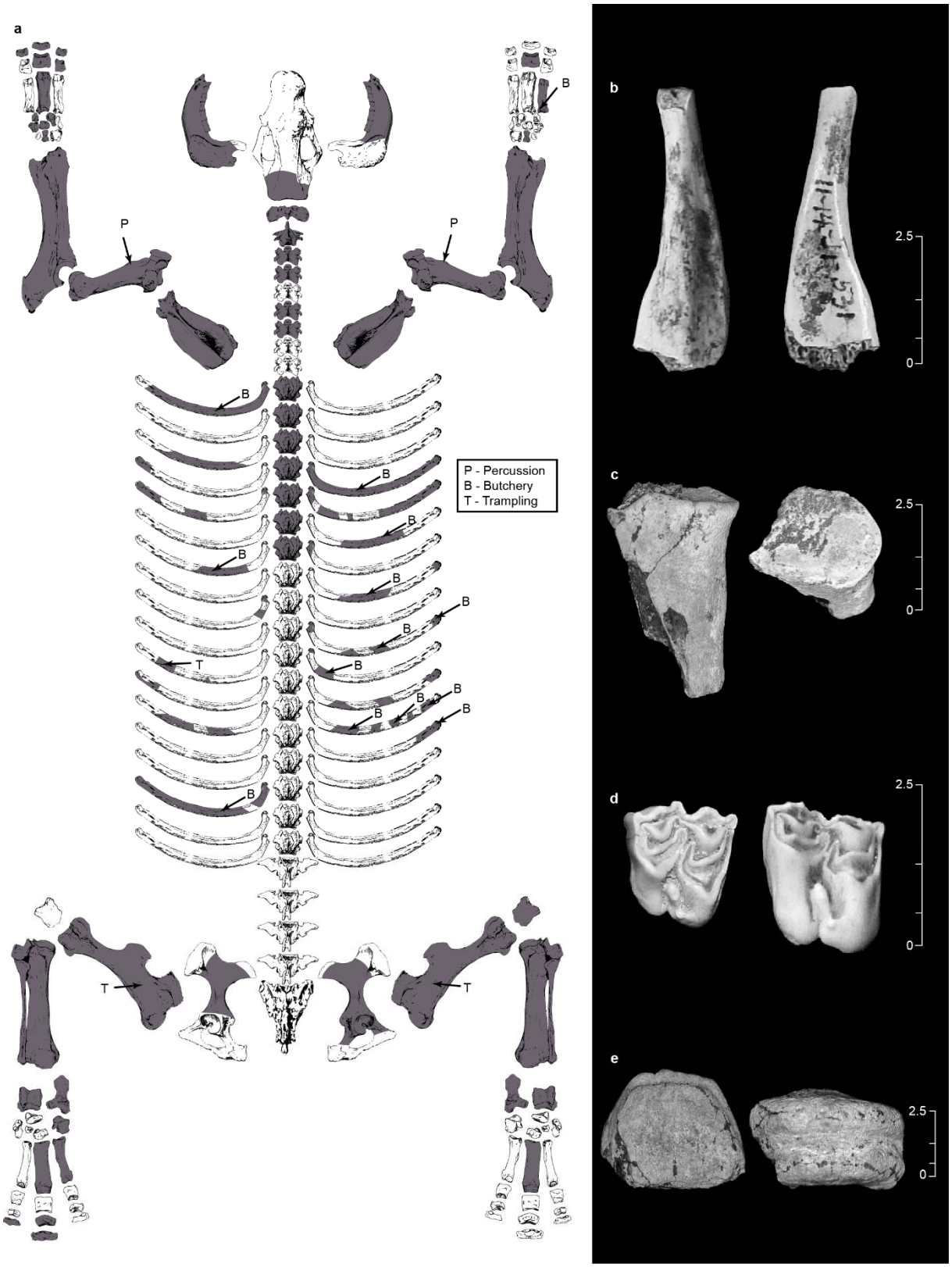

Extended Data Figure 2 | Faunal remains from Kalinga archaeological Unit F. a, Drawing showing the preservation of the rhinoceros and position of the taphonomical marks. A total of 97 fragments of ribs of all sizes have been recovered and not all of them could be clearly positioned on the skeleton. We estimate that about 75% of the skeleton has been recovered. **b,** Fibula of *Varanus salvator*. **c,** Radius of a Cervidae. **d,** Molar of *Cervus* cf. *mariannus*. **e,** Molar fragment of *Stegodon* cf. *luzonensis*.

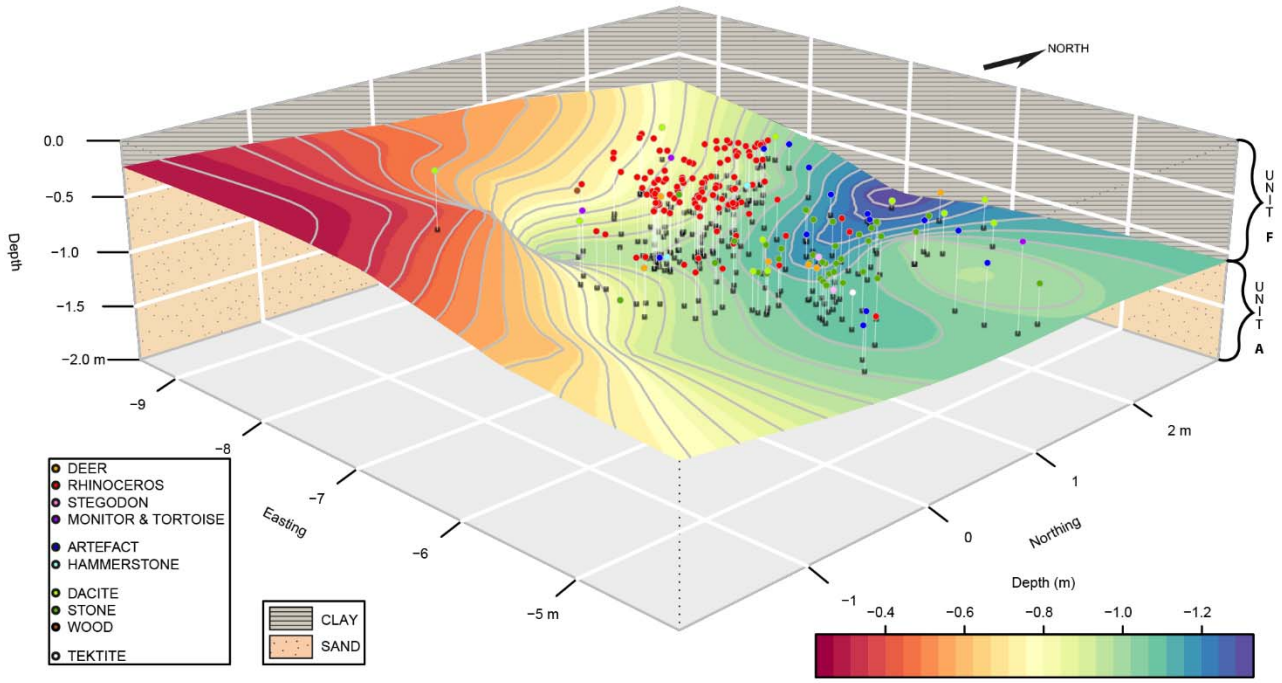

Extended Data Figure 3 | Digital Elevation Model (DEM) of the Main Kalinga Excavation, showing the contact surface topography between Unit A and Unit F and the vertical projections (black squares) of the archaeological materials (coloured points) on this surface. This DEM has been produced by interpolation through a kriging method from 37 three-dimensional coordinates recorded in the Main Excavation with a Total station on the erosional surface that cuts down into Unit A. This surface of contact corresponds to an erosional channel cutting down into sandy Unit A. All the material has been recovered lying across the base of the clayey Unit F along this channel, between 0.7m and 1.3m deep.

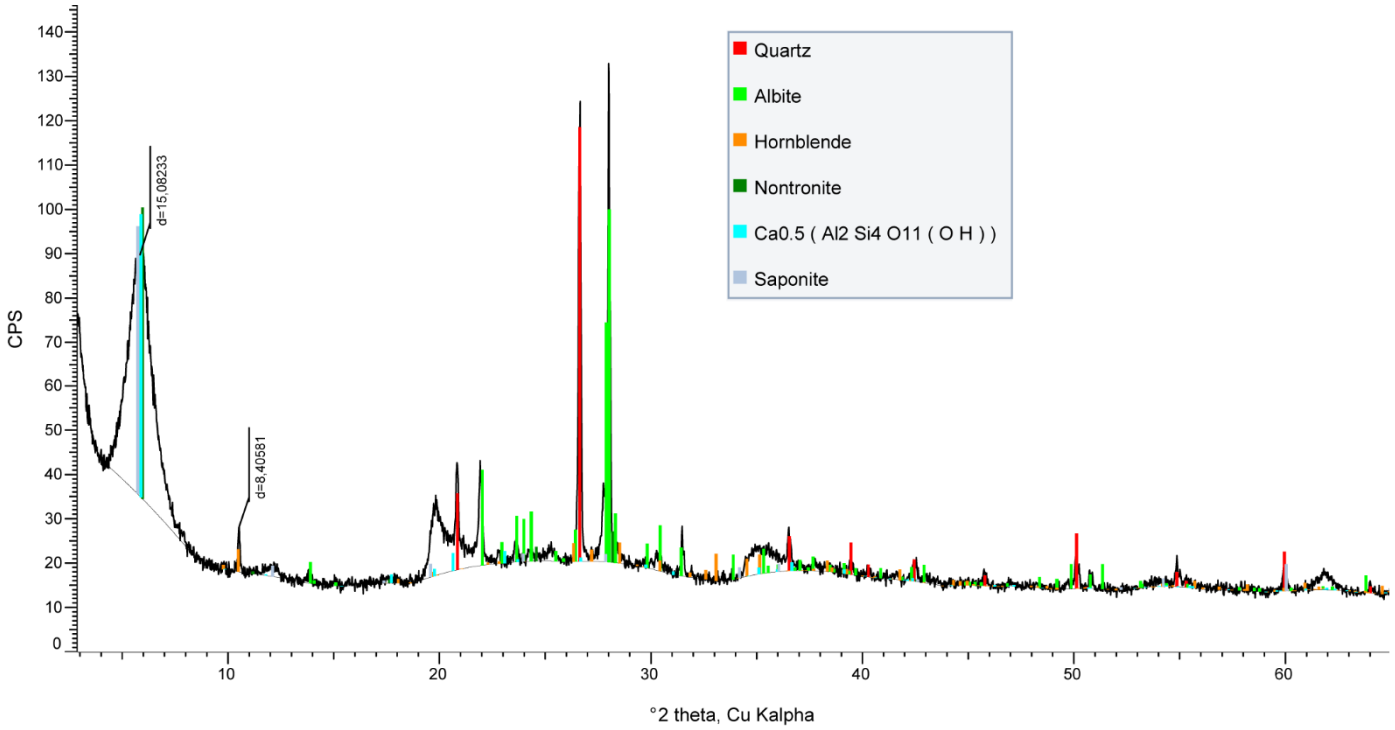

Extended Data Figure 4 | X-ray diffraction pattern of powdered Unit F clays. CPS is counts per second. Cu K-alpha corresponds to the wavelength. Quartz corresponds to the bipyramidal quartz crystals, some of which are visible to the naked eye. Bipyramidal quartz, albite, hornblende, nontronite and saponite all have a volcanic origin. Albite are plagioclase feldspar frequent in pegmatites. Hornblende is a common silicate mineral in igneous and metamorphic rocks. Nontronite is an iron-rich smectite type of clays which can be produced by hydrothermal alteration. Similarly, the smectite mineral saponite results from alteration of volcanic glass. The mineral composition of Unit F supports the interpretation as a mudflow set in a volcanic environment.

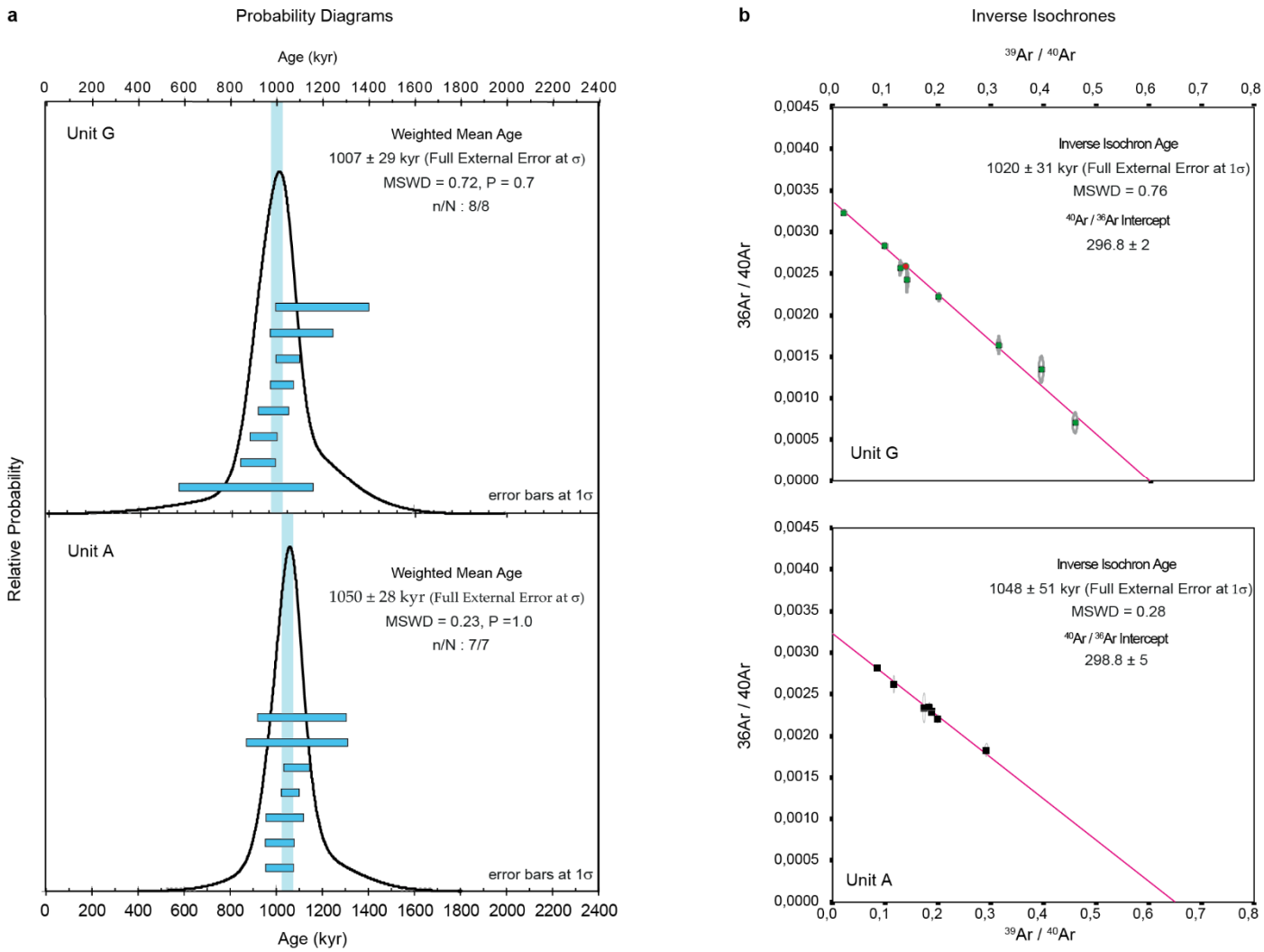

Extended Data Figure 5 | $^{40}Ar/^{39}Ar$ fusion ages of single potassium feldspar crystals for samples from Unit A and Unit G, presented as probability diagrams (**a**) that are correlated to the related inverse isochrones (**b**). Individual ages in **a** are ± 1σ.

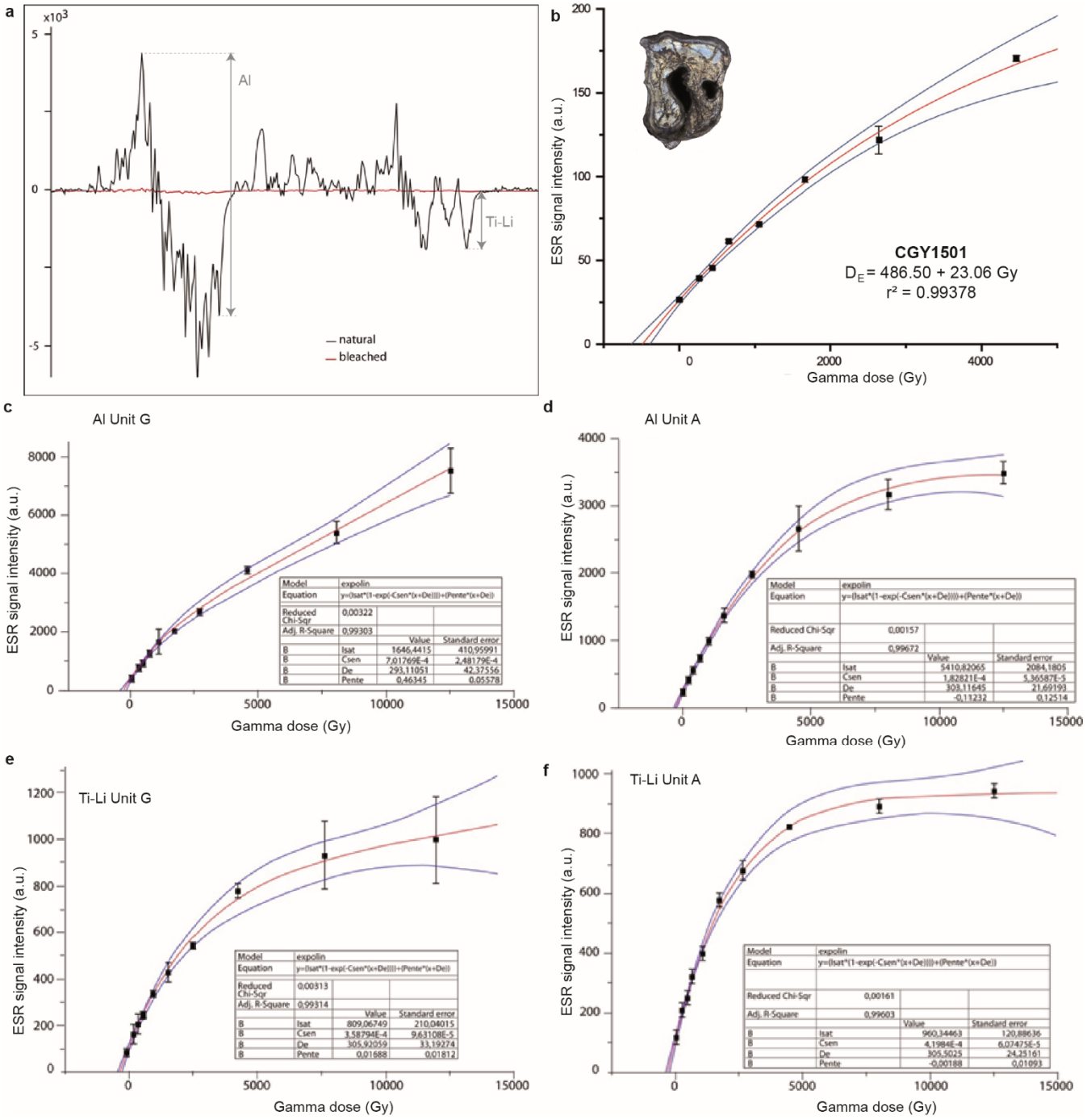

Extended Data Figure 6 | Measurements of dose rates (Da) and calculation of equivalent dose (De) to compute the ESR ages from quartz crystals and tooth enamel. a, Al and Ti centre ESR spectra of natural and bleached aliquots for Unit A quartz showing that Al signal is not totally reset although not measurable because extremely weak and covered by noise. **b**, ESR Dose-response curve obtained for the rhinoceros tooth (Archaeological number: II-2014-J1-095; sample code: CGY1501). The equivalent dose (D_E) was extrapolated using a single saturating exponential function (Origin Microcal software) following the recommendations of Duval and Grün[9] (D_E< 500 Gy, so D_{max}< 5000Gy for this sample). Vertical bars account for the standard deviation around the mean for each measurement. The red curve is for the dose-response curve. The blue curves account for the 95% confidence interval of the dose-response curve. **c-f**, ESR Dose Response curves, for Aluminium (Al) and Titanium-Lithium (Ti-Li) centers of layers G_1 and A_4. Vertical bars account for the standard deviation around the mean for each measurement. The red curve is the dose-response curve. The blue curves account for the 95% confidence interval of the dose-response curve.

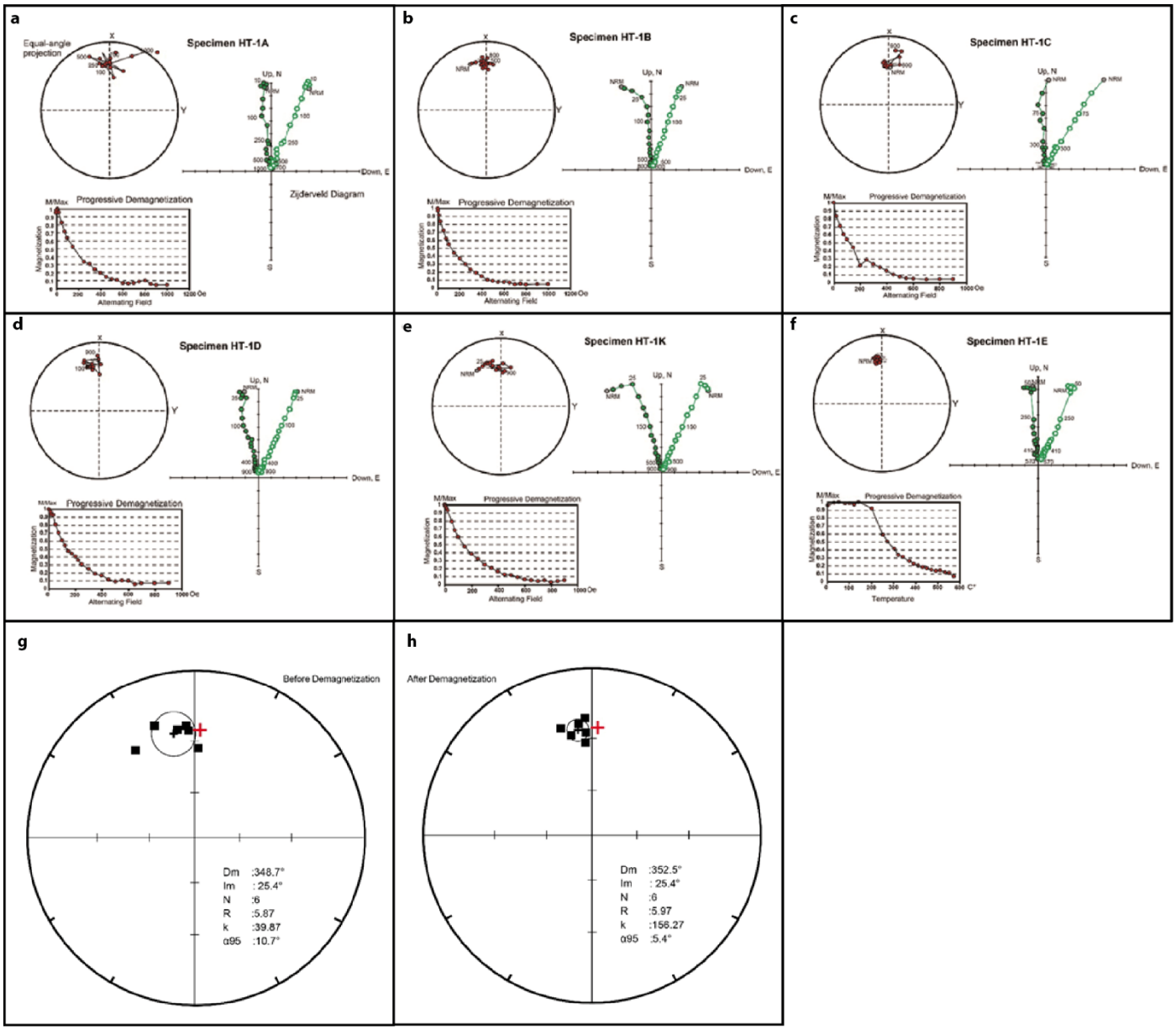

Extended Data Figure 7 | Progressive demagnetization curves (lower left of each panel), equal area projection stereoplots (upper left) and Zijderveld diagrams (right) for the six analysed specimens from Layer G_2. a-e: specimens treated by alternating field demagnetization; **f**, specimen HT-1E treated by thermal demagnetization. Open circles in the Zijderveld diagrams represent the inclination while closed circles represent declination. Open and closed circles in the equal area projection (stereoplot) represent the upper and lower hemisphere, respectively. Equal-area projections of the mean ChRMs directions of all analysed specimens, **g**, before and **h**, after demagnetization. Solid squares represent the upper hemisphere. Black cross indicates the mean ChRMs direction of the six specimens combined, surrounded by the α95circle. Red cross represents the present-day magnetic direction.

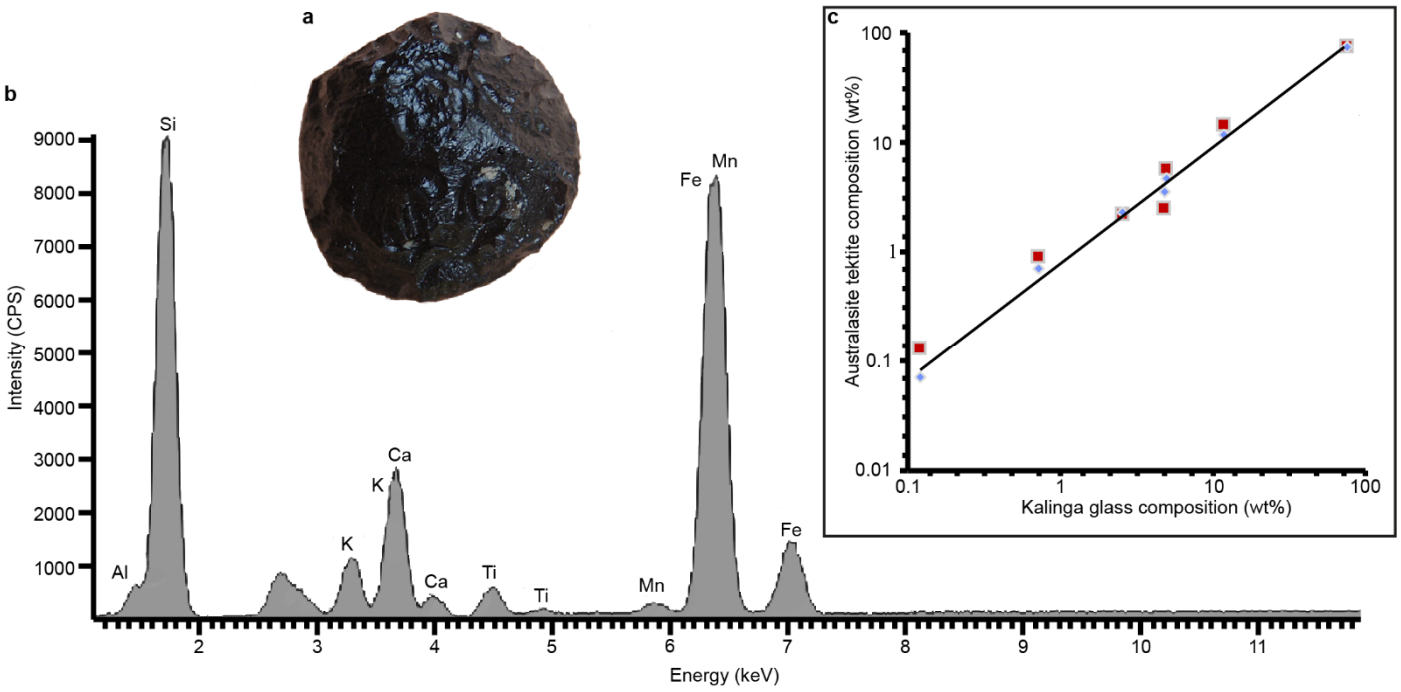

Extended Data Figure 8 | Analysis of the Kalinga tektite recovered from the archaeological layer Unit F. **a**, picture of the tektite: **b**, µXRF spectra (un-indexed peaks correspond to the Rh source) showing its composition: c, comparison of the Kalinga tektite glass composition through µXRF with an australasite tektite from China measured in the same conditions (red squares) and with an average australasite composition (blue diamonds) following Koeberl[50].

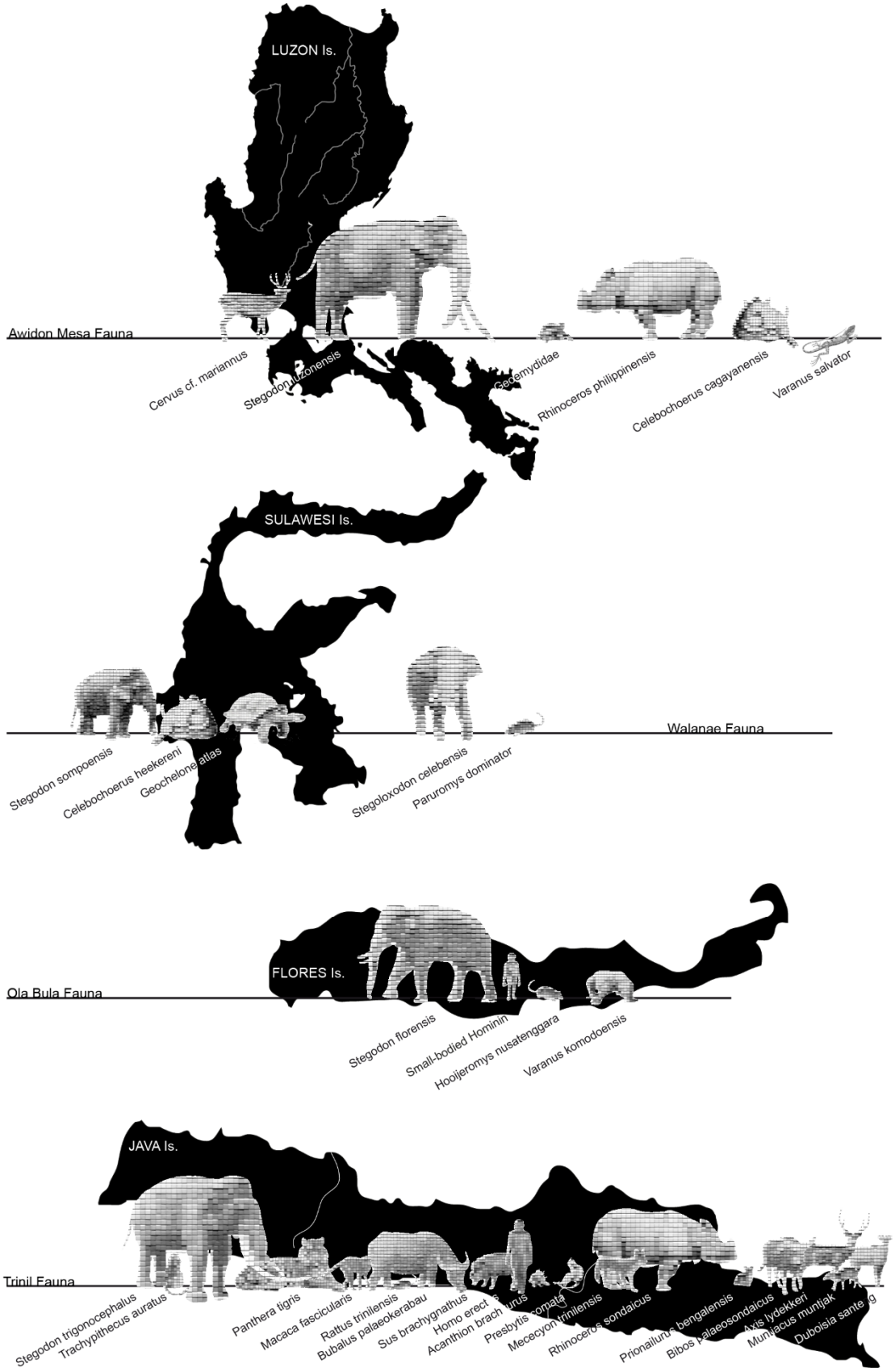

Extended Data Figure 9 | Fauna diversity of the Kalinga site as compared to contemporaneous faunas from other islands in the region. Contemporaneous to those faunas are 'classic' *Homo erectus* faunas on Java Island[97], the Mata Menge Fauna of Flores Island, which includes the putative ancestor of *Homo floresiensis*[98], and the Walanae Fauna on the southwestern branch of Sulawesi[99,100]

Extended Data Table 1 | ESR/U-series results for the rhinoceros tooth. a, U-series data for the tooth CGY1501. b, ESR/U-series data and age.

a

Sample	Tissue	U (ppm)	$^{234}U/^{238}U$	$^{230}Th/^{232}Th$	$^{230}Th/^{234}U$	$^{2220}Rn/^{230}Th$	Apparent U-series ages[1] (ka±2σ)
IPH-2015-09 CGY1501 (R-2014-J1-095)	dentine	52.3336 ± 0.1692	1.3701 ± 0.0062	141.40	0.8950 ± 0.0051	1.000	**220.70** ± 3.28
	enamel	0.2356 ± 0.0001	1.2564 ± 0.0009	48.96	0.8147 ± 0.0014	0.976	**164.86** ± 0.96

[1]Apparent U-series obtained for dental tissues should be regarded as minimum age estimates

b

Sample	Tissue	Palaeodose D_E (Gy)	U uptake parameter p	D_{α} Internal [1] (µGy/a)	$D_{\beta 1}$ [2] (µGy/a)	$D_{\beta 2}$ [2] (mGy/a)	$D_{(\gamma+cosm)}$ [3] (µGy/a)	D_s total (µGy/a)	ESR/U-series ages US [4] (ka±1σ)
IPH-2015-09 CGY1501 (R-2014-J1-095)	dentine	486.50 ± 23.06	-0.1636 ± 0.0893	47 ± 8	208 ± 35	50 ± 4	387 ± 16	692 ± 38	**709 ± 58**
	enamel		0.3834 ± 0.1530						

Eventual radium and radon losses from the dental tissues were estimated from cross-checked γ and α data[101]. Dose conversion factors of Guérin and co-authors[25] were used. Water contents of 0±0%, 7±5% and 10±5% were used for enamel (fixed), dentine (fixed) and sediments (difference in mass between the natural sample and the same sample dried for a week in an oven at 50°C) respectively.

[1] A k-value of 0.13 ± 0.02 was used following Grün and Katzenberger-Appel[102].

[2] The enamel thickness removed during preparation process was taken into account in the beta contribution calculation[103]. The following values were used for the age calculation: 1505±376µm, 351±88µm and 45±12µm for the initial thickness, thickness after preparation on the dentine side and on the sediment side respectively.

[3] Cosmic dose was estimated from depth using the Prescott and Hutton's formulae[30]. Because we have at present no means to know precisely when the erosion took place and since when the archaeological material became buried under less than 7m of sediment, a depth of 2.75m was used for the cosmic dose rate estimation as an intermediate value between the 7m of sediments that once covered the archaeological layer and the present 70cm to 1.20m depth at which the archaeological material was recovered, and as an average between the once full thickness of the archaeological layer and its present thickness where the archaeological material was recovered. A cosmic dose estimated from a depth of 7m would result in a 10% older age for the Unit F and a cosmic dose estimated from a depth of 1m would result in a 7% younger age for the Unit F.

[4] Uncertainties on the ESR/U-series ages were calculated using Monte-Carlo approach following Shao and co-authors[104]

SUPPLEMENTARY INFORMATION

Excavation methods.

The Main Excavation comprises four 2x2 m quadrants arranged in 'T' shape (Extended Data Fig. 1). Excavation took place in 10-cm spits, separating the sediments from distinct stratigraphic layers where appropriate. The excavation was undertaken with bamboo sticks to prevent damage to the fossils and stone artefacts. All sediments were dry and wet sieved. The first quadrant was dug in 2014 at the site where a concentration of fossils and stone artefacts was found on the surface, including a *Celebochoerus cagayanensis* canine fragment[1]. This quadrant, referred to as the test excavation or South Quadrant (S-Q), had reached a depth of 1.2 m when the first rhinoceros fossils were found embedded in a silty clay plug that had filled in an ancient channel with a sandy bottom. The trench was then extended with two 2x2 m quadrants adjacent and directly to the north and northwest of S-Q. (N-Q and NW-Q, respectively). More fossils of a single rhinoceros skeleton and also stone artefacts were excavated along the same erosive contact between a sandy channel base (Unit A) and a clayey channel fill deposit (Unit F). From the southern baulk of S-Q a 1 m wide connection with slot Trench H was made to examine the continuation of sedimentary layers in the Main Excavation and Trench H.

In 2015 the Main Excavation was further extended to the east with a 2x2 m quadrant (NE-Q) east of N-Q, in order to trace the fossil bearing horizon in an eastern direction, and to expose a larger area of the undulous fossil-bearing surface. Also, S-Q was excavated further to a maximum depth of 1.8 m to examine a larger portion of the sandy layers (Unit A) below the fossil-bearing horizon.

The three-dimensional coordinates of all artefacts and fossil bones (Extended Data Fig. 3) (and the orientation, dip and plunge of long bones) were recorded with a Leica© Total station. The rhinoceros bones where retrieved one by one after having been first protected with a layer of petroleum jelly, a layer of plastic bags and an outer layer a plaster of Paris armed with bamboo sticks to consolidate the samples for transport. Fine cleaning with water and a soft brush and consolidation of the bones with a 20% paraloid B72 solution was achieved in the zooarchaeology laboratory of the Archaeological Studies Program of the University of the Philippines Diliman using a magnifying glass.

Sedimentology

Stratigraphically, the site layers pertain to the upper part of the Awidon Mesa Formation, a Pleistocene sequence of alluvial stream deposits intercalated with volcaniclastic and pyroclastic deposits. The depositional environment of the Awidon Mesa Fm was characterized by braided rivers on an alluvial fan system that formed in response to uplift in the Cordillera Central to the West[2,3]. The apex of this fan was near the point where the present paleo-Chico River Valley widens into the Cagayan Valley (West to the Pangul Anticline) (Fig.1). During periods of volcanic activity in the catchment area of the Chico River, large amounts of pyroclastic flows and lahars were fed onto this alluvial fan system. The ignimbritic layers are characterized by a dacitic composition, and one of the defining characteristics

of the Awidon Mesa Fm is the occurrence of reworked bipyramidal volcanic quartz crystals in the clastic sediments. Continued east-west compressional deformation led to the uplift of the Pangul Anticline to the South and West of the excavation area, as well as the Cabalwan and other north-south trending anticlines in the Cagayan Valley. This deformation phase is thought to have redirected the Chico River to the north in its present-day configuration, thus bringing deposition on the westward prograding alluvial fan system as exposed in the Cabalwan Anticline, to a halt.

The Kalinga site layers were grouped into stratigraphic units based on differences in texture, sedimentary structures, and consolidation, where each unit was thought to represent common facies associations indicative for specific depositional environments. Samples were taken for grainsize analysis from the baulks of the Main Excavation and Trench H (Extended Data Fig. 1).

Grainsize analyses were performed at the sedimentology laboratory of the School of Earth and Environmental Sciences at the University of Wollongong, Australia. Small amounts of each sample were put in plastic flasks with distilled water, which were then placed in an ultrasonic bath to loosen the sediment over a period of 2 hrs. The samples were then sieved through 1 mm mesh and analysed with a Malvern Mastersizer 2000©. The minerals content of the archaeological layer Unit F was obtained from X-ray Powder Diffraction (XRD) on 30g sub-samples placed into a Brucker© D2 Phaser diffractometer at the UMR 5143 laboratory of the Muséum National d'Histoire Naturelle in Paris, France. The occurrences of crystal minerals in the fossiliferous clay were identified by matching the XRD pattern with reference patterns of pure substances (Extended Data Fig. 4).

The fossiliferous clay (Unit F) unconformably overlies a coarse to medium sandy, indurated fluvial layer (Unit A) with cross bedding and scour and fill structures. A concave channel has cut down into this fluvial unit. Fossils and stone artefacts were found concentrated directly above the deepest part of the erosional surface, and are embedded in and covered by a massive, very poorly sorted fine-grained mudflow layer (Unit F), which has filled in the channel (Extended Data Figs. 1 & 3). This archaeological layer is a very poorly sorted, up to 3.25 m thick, muddy unit. In the Main Excavation, Unit F is cut by the modern topography and a 10 to 60 cm thick recent topsoil has overprinted the interval directly beneath the ground surface. Unit F is made up of predominantly silty clay with variable admixtures of sand – including slightly rounded bipyramidal and non-euhedral quartz– and rounded pebbles, which are predominantly dacites. The XRD spectrum of the fossiliferous clay points to a high concentration of volcanic-derived minerals including saponite, which often forms as a result of the alteration of volcanic glasses[4,5] (Extended Data Fig. 4). The overall very poor sorting (Extended Data Fig. 1) indicates that Unit F was deposited by a mudflow filling in a pre-existing fluvial channel (most probably following a volcanic eruption), which is further substantiated by the higher concentration of pebbles in the lower part of Unit F and the absence of pollen.

We applied three different geochronological methods, each of which are based on different physical principles. $^{40}Ar/^{39}Ar$ dating was performed on plagioclases from Unit A and Unit G and Electron Spin Resonance (ESR) dating was applied to bipyramidal quartz crystals from these same two units. Thirdly,

Uranium-Thorium ESR (ESR-U/Th) dating was applied to rhino fossil tooth enamel recovered from Unit F. The results obtained for each method account for different geological processes. In the case of $^{40}Ar/^{39}Ar$, the obtained ages correspond to the crystallization age of the plagioclases. Since the sedimentary units from which the crystals were extracted are not primary voclanoclastic deposits but instead fluvial layers, the true depositional ages of these units must be younger than the Ar-Ar ages we obtained [6]. Therefore, they provide a maximum age for the sedimentological formation from which they have been extracted. In contrast, ESR applied on optically bleached quartz provide the age of deposition of the sedimentary quartz subsequent to their transportation, which resulted in resetting their geochronometer[7]. The ESR-U/Th dating method on the fossil rhino tooth dates the death and burial of this animal within the sedimentary unit. Furthermore, the geological age of death of the rhinoceros corresponds to the age of the apparent butchery marks on its bones. Therefore, the age of hominin presence in Kalinga site is given by the ESR-U/Th age of 709±68, and is bracketed by the ESR on quartz ages obtained on the underlying and overlying sedimentary units, which are between 727±30 and 701±70, respectively. It would be expected that the $^{40}Ar/^{39}Ar$ ages provide older ages, which correspond to a volcanic eruption after which the crystal minerals were reworked into the sedimentary units. Therefore they provide a maximum possible age for the site. These different geochronological methods as applied to different archaeological materials are all coherent with deposition of the fossils and artefacts just after the Brunhes-Matuyama boundary, which is further substantiated by the palaeomagnetism results and the presence of a reworked Australasian tektite in the bone-bed Unit F.

Combined ESR and U-series dating on tooth enamel

A combined Electron Spin Resonance (ESR) and Uranium-series (U-series) approach was applied on a rhinoceros' right maxillary third premolar (Archaeological number: II-2014-J1-095; sample code: CGY1501) excavated from the archaeological layer Unit F, following the protocol described by Bahain and co-authors[8]. After mechanical separation of the dental tissues, the enamel was cleaned using a dental drill to remove any contamination of sediment or dentine. For the calculation of the beta contribution, the initial enamel thickness was measured to 1505±376 µm, and, following enamel preparation, the removed thickness was measured to 351±88 µm on the dentine side and 45±12 µm on the sediment side. The enamel was then ground and sieved. The 100-200 µm fraction was used for equivalent dose (D_E) determination: it was split in ten aliquots, nine of them were irradiated by a γ 60Co source at doses ranging from 260 to 12500 Gy. The ESR intensity of each aliquot was then measured using a Bruker© EMX ESR spectrometer and a dose-response curve was built from the data set for the tooth. D_E were determined using a single saturating exponential function from the eight first aliquot intensities according to the protocol proposed by Duval and Grün[9] (Extended Data Fig. 6). Radioelement contents of the dental tissues and associated sediments were measured by γ-ray spectrometry and U-series were performed on each dental tissue. The γ dose was measured in the laboratory from three sediment samples taken from the homogeneous clayey Unit F at proximity of the analysed tooth and the obtained value

has been combined with the γ dose measured *in situ* from sandy Unit A as this underlying sedimentary layer contributed for a small amount to the total dose received by the tooth as observed on the site. Therefore, the γ dose used for the calculation of the age from the tooth combined 5% of the γ dose from layer A3, 65% from layer F1 and 30% from layer F2 (Extended Data Figure 1a).

The uranium (U) and thorium (Th) isotopic analyses on the dental tissues were performed on a Neptune© Multi-Collector Inductively Coupled Plasma Mass Spectrometer (MC-ICPMS) at Nanjing Normal University, Republic of China. The chemical protocol used for sample preparation follows the method described by Shao and co-authors[10]. The uranium and thorium fractions were separated from each other and from the matrix material using some UTEVA® resin columns and were dissolved in a mixture of 0.1N HNO3 and 0.01N HF for MC-ICPMS analysis. The radioelements content of the sediments are listed in Supplementary Information Table 2. No ^{238}U decay chain was observed. Uranium was measured statistically by ^{233}U, ^{235}U, ^{236}U and ^{238}U on Faraday cups and ^{234}U simultaneously on a secondary electron multiplier (SEM). Thorium was analysed with ^{230}Th and ^{229}Th alternately on the SEM and ^{232}Th on a Faraday cup. The uranium isotopic ratios of the standard uraninite HU-1 were measured before and after each uranium and thorium isotopic measurement. Mass fractionation was corrected by comparing the measured ^{238}U/^{235}U to the value of 137.760 for the HU-1 standard and to the value of 137.818 for natural samples[11] with an exponential law. The mass fractionation for uranium and thorium are assumed to be equivalent. The SEM to Faraday cup yield was assessed by the δ^{234}U measured in the HU-1 standard. Hydride interferences, machine abundance sensitivity and amplifier gains were evaluated every day prior to sample measurements. The ^{230}Th/U ages were calculated using half-lives of 75,584 years and 245,620 years for ^{230}Th and ^{234}U, respectively[12]. The ESR-U/Th ages were calculated with the "ESRUS" Matlab software written by Qingfeng Shao[13]. Lastly, dose rates (D_a) contributions, U-uptake parameters and ESR/U-series ages were calculated applying the classical US model[14], which provided an age of 709 ± 68 (1σ) ka for the rhinoceros tooth. These results are presented in Extended Data Table 1.

ESR dating on fluvial quartz

ESR dating was applied on fluvial quartz grains collected from two samples, one taken in Unit A (Layer A_4) and the other one in Unit G (Layer G_1) encapsulating the archaeological bone-bed Unit F. The volcanic bipyramidal quartz crystals from Unit F were also analysed but did not return any exploitable result due to their shape (not reducible into powder), size and strong angular dependence. The ESR method is based on the measurement of the accumulated natural radiation dose resulting from environmental radioactivity[15]. ESR dating of quartz uses radiation sensitive paramagnetic centres such as aluminium or titanium[16,17] and relies on the resetting of any previously present signal by sun light exposure at the time of deposition[7]. An age is derived by assessing the total dose received by the sample since its deposition divided by the dose rate which is obtained from all environmental radiation sources

including cosmic rays. The analysis was done at the Geochronology laboratory of the UMR 7194, Muséum National d'Histoire Naturelle of Paris, France.

Both ESR signals of the aluminum (Al) and titanium (Ti) centres were studied (Extended Data Fig.6 c-f). The extraction and preparation protocol of quartz grains is described in Voinchet and co-authors[18]. After extraction, each sample was split into eleven aliquots. Nine of them were irradiated with a γ 60Co source (Commissariat à l'Énergie Atomique, Saclay, France) emitting 1.25 MeV radiation with a dose rate of about 200 Gy/h. The nine additive doses are 264, 431, 653, 1048, 1663, 2640, 4460, 8010, 12500Gy. One aliquot was conserved as natural reference and the eleventh aliquot was exposed during 1600h to light in a Dr Honhle© SOL2 solar simulator (light intensity between 3.2 and 3.4 105 Lux) in order to determine the unbleachable portion of the ESR-Al signal. Each series of eleven aliquots was measured at least three times by ESR at 107K using a Bruker© EMX spectrometer and every measure of each aliquot was undertaken three times after an approximatively 120° rotation of the tube in the ESR cavity, in order to consider angular dependence of the signal due to sample heterogeneity.

For the aluminium ESR centre study, the acquisition parameters used were : 5 mW microwave power, 1024 points resolution, 20 mT sweep width, 100 kHz modulation frequency, 0.1 mT modulation amplitude, 40 ms conversion time, 20 ms time constant and 1 scan. The signal intensity was measured between the top of the first peak at g=2.018 and the bottom of the 16th peak at g=2.002 of the Aluminum hyperfine structure[18]. For the Titanium centre, the acquisition parameters used were : 10 mW microwave power, 1024 points resolution, 20 mT sweep width, 100 kHz modulation frequency, 0.1 mT modulation amplitude, 40 ms conversion time, 20 ms time constant and 2 scans. The signal intensity was measured using the Ti-Li option D[20]. Equivalent doses (D_E) were then determined from the obtained ESR intensities versus the dose growth curves using a coupled exponential and linear function[21,22] with Microcal OriginPro 8 software with $1/I^2$ weighting. In the age calculation, the dose rates D_a were calculated from the radionuclides contents of the sediments and taking into account the *in situ* gamma-rays data and the location of the samples in the stratigraphic sequence.

The dose rate (D_a) provided by the sediment surrounding the sample was obtained from the sum of the alpha, beta, gamma and cosmic-ray contributions. We have at present no means to know precisely when the erosion took place and since when the archaeological material became buried under less than 7m of sediment. Therefore, a depth of 2.60m, which is the thickness between the base of layer A4 and the top of layer G1 still covering Unit A and F where the sample was taken, was used for the cosmic dose rate estimation of Unit A. A depth of 3.40m was used for the cosmic dose rate estimation of Unit G which corresponds to the thickness measured between the base of layer G1 and the laminated silty layer J4 considering that part of Unit J still covers Unit G where the sample was taken. A cosmic dose estimated from a depth of 7m would increase the age for the Unit A by 13% and by 16% for Unit G. Gamma dose rate was determined by *in situ* measurements using an Ortec Digidart LF gamma spectrometer (Canberra©). These gamma doses were estimated using the threshold approach[23]. External alpha and beta contributions were calculated from the sediment radioelement contents (U, Th and K) as

determined in the laboratory by high resolution and low back ground gamma-spectrometry[24]. Age calculations were performed using the dose-rate conversions factors from Guérin and co-authors[25], a k-value of 0.15 ± 0.1 [7,26], alpha and beta attenuations from Brennan and co-authors[27,28], water attenuation formulae from Grün[29] and a cosmic dose rate calculated from the equations of Prescott and Hutton[30]. Because the analyzed sediments are of fluvial origin deposited under tropical conditions, the water content should have never been less than 10%. Furthermore, because the analyzed sandy sediments do not show any large hydromorphic features, the water content should have never been higher than 20% which is the field capacity for fine sandy loam[31]. The measured water content of Unit A and G, respectively 15% ± 5 and 13% ± 5, are in accordance with these expected parameters and were used for calculation of the ages. Our calculations show that an increase in assumed water content from 10% to 20% would result in an increase in the calculated mean age of 12 to 14% for both sandy units. The internal dose rate was considered as negligible because of the low contents of radionuclides usually found in quartz grains[32,33]. ESR age estimates are given with one sigma error range.

During the analysis of the samples, an unusual behaviour of aluminum ESR centres was observed, consisting in a total resetting of the signal after the laboratory bleaching simulation, which is more usually observed for titanium centers. The Al bleach aliquot signal is therefore not measurable as it is obliterated by noise (Extended Data Fig. 6 a). This noise might be due to the presence of silica in a different structure than alpha quartz within the sediments. The analyzed quartz appears to be very smooth bi-pyramidal quartz. Here the aluminium and titanium centres showed the same behaviours under bleaching which lead to close D_E values for the two centres (Extended Data Fig. 6 c-f). Observation of this similarity during the bleaching process encouraged consideration of a weighted average age for each stratigraphic layer.

The weighted average ages were calculated using IsoPlot 3.0[34] and given at 95 % probability including *J* uncertainty. Weighted mean ages are 727 ± 30 ka (1σ, Full external uncertainty, Mean Square Weighted Deviation (MSWD) = 0.013 and Probability fit (P) = 0.91) for unit A and 701 ± 70 ka (1σ, Full external uncertainty, Mean Square Weighted Deviation = 0.18 and Probability fit = 0.67) for unit G. These dates bracket the age of the archaeological remains (Supplementary Information Table 1).

Argon/Argon dating

Two sandy layers, Unit A (Layer A_4) and Unit G (Layer G_1) were selected for the laser fusion $^{40}Ar/^{39}Ar$ single-crystal dating method. After crushing and sieving, feldspars ranging from 500 μm up to 1 mm in size were handpicked under a binocular microscope and then slightly leached for 5 minutes in 7% HF acid. A total of thirty crystals were handpicked after leaching and eight of them were separately loaded in a single aluminium disk for each sedimentary Unit. The samples were irradiated for 60 minutes (IRR 106) in the β1 tube of an OSIRIS reactor (Commissariat à l'Énergie Atomique, Saclay, France). After irradiation, the samples were transferred into a copper sample holder and then loaded individually into a differential vacuum Cleartran© window. Crystals were individually fused using a

Synrad CO2 at 10-15 % nominal power (c.a 25 W). The Ar isotopes were counted using a VG5400 mass spectrometer equipped with a single ion counter (Balzers© SEV 217 SEN), following the procedures outlined in Nomade and co-authors[35]. Each Ar isotope measurement consisted of 20 cycles of peak switching of the argon isotopes. Neutron fluence (*J*) was monitored by co-irradiation of Alder Creek sanidine (ACs-2 [36]) that were placed in the same pit as the sample during irradiation. The *J* value for each sample was determined from analyses of two ACs-2 single crystal measurements. The corresponding *J* values were calculated using ACs-2 at 1.185 Ma[37], the total decay constant of Min and co-authors[38] and the $^{40}Ar/^{36}Ar$ atmospheric ratio of 298.56 [39]. Procedural blanks were measured every two or three unknowns, depending on the sample beam size previously measured. For a typical 9-min static blank, the backgrounds were generally between 2.0–2.2 × 10^{-17} and 5.0–6.0 × 10^{-19} mol for ^{40}Ar and ^{36}Ar, respectively. The precision and accuracy of the mass discrimination correction was monitored by weekly measurements of various beam sizes of atmospheric air (see Nomade and co-authors[34], for full experimental description). Individual crystal measurements, *J* values as well as nucleogenic production ratios used to correct for reactor-produced Ar isotopes from K and Ca are reported in Supplementary Information Table 3 and 4.

For the two investigated sedimentary layers (Unit A and Unit G) the probability diagrams were simple and point towards one single homogeneous crystal population identical within uncertainties allowing us to calculate a valid weighted mean age. A population is considered to be relevant when the weighted mean age of these crystals present the following statistical characteristics: MSWD (Mean Square Weighted Deviation) < 1.5, Probability fit ≥ 0.1. These weighted average ages are calculated using IsoPlot 3.0 [40] and given at 95 % probability including *J* uncertainty throughout the text. *J* values are: $J = 3.2730.10^{-4} \pm 0.00000098$ and $J = 3.3420.10^{-4} \pm 0.00000201$, for Unit A and G respectively. Weighted mean ages are 1050 ± 28 ka (1σ, Full external uncertainty, MSWD = 0.23 and P = 1.0) and 1007 ± 29 ka (1σ, Full external uncertainty, MSWD = 0.72 and P = 0.7) for Unit A and Unit G, respectively. No excess argon was highlighted by the inverse isochrones that both present a $^{40}Ar/^{36}Ar$ initial intercept (i.e. 296.8 ± 4 and 298.8 ± 9; 2σ) equivalent within uncertainties to the atmospheric ratio[39]. The full data can be found in the Extended Data Fig. 5 and Supplementary Information Table 4**.**

Palaeomagnetic dating

An oriented block sample for palaeomagnetic dating purposes was obtained from the north baulk of Trench H south of the Main Excavation (Fig. 1; Extended Data Fig. 1). Due to the scarcity of suitable undisturbed fine-grained layers only one stratigraphic layer was sampled. The sample was taken from a 15-20 cm thick, well-sorted, laminated silty layer exposed in the lower part of Unit G (Layer G_2). The sample was taken using a cubic, sealable plastic container of 10x10x10 cm, fitted over a cube-shaped pedestal that was carved to fit the container. The block sample was tightly sealed and oriented using a Brunton compass, corrected for local declination, and transported to the Centre for Geological Survey in Bandung, Indonesia, for further analysis. All treatments and measurements were performed in the

magnetically shielded room at the Palaeomagnetic Laboratory in the Centre for Geological Survey. Six cube-shaped sub-samples or specimens, each with a volume of ~10 cm^3, were cut from the block sample. Magnetic Remanence directions of the specimens were determined using two different methods. Five specimens (HT1A-D and HT-1K) were demagnetized using Alternating Field (AF) using a Schonstedt© GSD-1 AF demagnetizer, with intervals of 0.5, 1, 2.5, and 5 mT, up to peak fields of 90-100 mT. A single specimen (HT-1E) was demagnetized using a MMTD-80 Thermal Demagnetizer© (TD), with intervals of 20º C, 30º C to 50º C up to a maximum of 580° C. Direction and intensity measurements were performed using a AGICO© JR-6A Spinner Magnetometer.

Progressive demagnetization curves, stereoplots and Zijderveld diagrams of all the six analysed specimens are shown in Extended Data Fig. 7 a-e. The Zijderveld diagrams show that most specimens appear to have only a single Natural Remanent Magnetization (NRM) component. Only two specimens (HT-1B and HT-1K) had a secondary magnetic component, which was easily removed. The stereoplots demonstrate that all specimens show little change in NRM direction during stepwise demagnetization. This could indicate a very strong secondary magnetization that influenced all specimens. However, progressive alternating field demagnetization at 50 – 60 mT reduced the intensity to only ~10% of the total intensity before demagnetization, showing that secondary magnetization was eliminated and Characteristics Remanent Magnetizations (ChRMs) was acquired. All ChRMs progressed to the origin of the orthogonal vector projections at higher field strengths.

To further test that the ChRMs were successfully isolated, one specimen was demagnetized using TD (specimen HT-1E). The TD treatment also resulted in a single magnetic component with little change in the NRM direction during progressive heating up to 580º C, when magnetic intensity was reduced to ~10 % of the total intensity prior to demagnetization (see Extended Data Fig. 7-f).

Supplementary Information Table 5 shows the magnetic intensities of all six analysed specimens before and after intensity saturation was achieved, as well as the mean ChRMs directions for each specimen. Mean ChRMs directions were determined using Puffin Plot Software[41] and super IAPD 2000 that uses principal component analysis[42] and calculates site and mean directions following Fisher[43]. The maximum angular deviation was set at < 5°. The mean ChRMs direction of the six specimens combined was close to the present-day Normal polarity (Dm = 352.5°, Im = 25.4°; Extended Data Fig. 7 g-h). Applying the criteria for palaeomagnetic data reliability of Butler[44] this outcome is reliable (R = 5.97, k = 156.27, $\alpha 95$ = 5.4°).

Non-destructive characterization of the tektite

The earliest records of tektites recovered from the Philippines were from Rizal Province, Northeast of Manila, and were described by Henry Otley Beyer in 1928. Beyer was an anthropologist and archaeologist from the University of the Philippines, and, in 1962 published a book covering his collected papers on the topic. Following this publication, all tektites from the Philippines were referred to as rizalites, and all present similar physical characteristics resulting from brittle spalling. Rizalites

chemical signatures are also identical to the other tektites originating from the Australasian strewn field, an impact that took place somewhere between Southern China and the Bay of Tonkin west of the Cagayan Valley 786+/-2 ka ago[45].

Visual inspection of the black glass recovered from the Unit F bone-bed (Extended Data Fig. 8a) reveals a near spherical ellipsoid of 9.43 g, with surface aspects and ornamentation typical of tektites (Extended Data Figure 1f & 8a), and in particular those from the Philippines. The surface aspect shows no fluvial transport but there is evidence of etching by soil acid resulting from a long term residence in the sediment. The nearest source for obsidian from Kalinga is located 120 km to the Northwest where green glass is outcropping. Black obsidian in the Philippines is only known to the South of Manila[45]. Furthermore, no microcrystals, typical of obsidian, are observed in the Kalinga glass when examined in transmitted light under cross polarizer microscopy.

The field magnetic susceptibility (χ) of the Kalinga glass, measured with a MFK1 Agico Kappabridge, has a value of 77 $\times 10^{-9}$ m^3/kg while obsidian with χ below 100 are extremely rare, and usually not black. The measured value on the Kalinga glass is in good agreement with Australasian tektite data[45] which shows a range from 57 to 103 $\times 10^{-9}$ m^3/kg and an average of 82 ± 10 $\times 10^{-9}$ m^3/kg (n=152) according to the literature[46] and a mean of 87 ± 6 $\times 10^{-9}$ m^3/kg and a range from 69 to 129 $\times 10^{-9}$ m^3/kg based on our own measurements on a sample of 1500 specimens. The only other tektites within that range are from the Ivory Coast (1.1 Ma) and Texas (35 Ma)[47].

Saturation isothermal remanence magnetism (SIRM) shows that low susceptibility in obsidian is mostly due to ferromagnetic inclusions, which are unlike the paramagnetic iron diluting the tektite glass. While SIRM in tektites is usually below 10^{-6} Am^2/kg (maximum 4.10^{-6} Am2/kg [48]), SIRM in low susceptibility obsidian is above 10^{-3} Am^2/kg with the lowest measured value being above 10^{-5} Am^2/kg on samples from Lipari (Italy)[49]. The Kalinga sample yield an SIRM of $0.65.10^{-6}$ Am^2/kg (measured with a 2G cryogenic magnetometer after a 3 T field application), which is typical of tektites, including Australasites. This evidence serves to further exclude volcanic glass.

µXRF spectra obtained using a Horiba XGT700 instrument (30 kV, 100 µm spot, 200 s counting time) yielded the following major element semi-quantitative composition in wt.%: SiO2 75.2, Al2O3 11.7, Fe2O3 4.9, CaO 4.8, K2O 2.5, TiO2 0.71, MnO2 0.12 (Extended Data Fig. 8b). This composition is consistent with previous analyses, being at odds with an obsidian composition (which is characterized by lower Fe and higher K values). Comparison with a shard of Australasite from China measured under the same experimental conditions yielded comparable values except for CaO (Extended Data Fig. 8c). However, this variability is not exceptional in the Australasian strewn field, and the Kalinga CaO is within the 3.5% of average data published[50].

We conclude therefore, based on visual inspection, magnetic measurements and local geological context, that the Kalinga glass is a tektite belonging to the Australasian strewn field dated at 0.79 Ma[45]. Tektite strewn fields are very rare (four have been officially accepted, and two are under study from Central and South America), the Australasian field being by far the largest in the world, and the only

one from Asia. The possibility that the Kalinga sample belongs to another, unknown tektite strewn field rather than to the Australasian field is therefore unlikely.

The presence of an Australasian tektite in the bone-bed along with normal polarity palaeomagnetism in the sedimentary unit directly overlaying the bone-bed suggests an age for the fossil and archaeological remains of Kalinga site that is younger than the Lower-Middle Pleistocene boundary. This is in agreement with the ESR ages obtained on quartz from Unit A and G and on the fossil tooth enamel from Unit F. Because the ESR method is measuring the age of the last deposition of the fossils and sediments, we retain those dates when estimating the minimum age of the Kalinga site. In contrast, the $^{40}Ar/^{39}Ar$ method focuses on dating the origin of the volcanic plagioclase crystals and therefore represents a maximum age for the Kalinga archaeological site. The combination of the methods applied to different materials therefore constrain the age of the archaeological findings at Kalinga and suggest they are not older than 777 ka (ESR-U/Th on enamel lower tail probability at 1 sigma) and not younger than 631 ka (ESR-U/Th on Unit G quartz upper tail probability at 1 sigma).

Palaeobotanical analyses

A waterlogged wood fragment was found during the 2014 field season in the clayey matrix of the archaeological Unit F next to one of the ribs of the rhinoceros fossil (Extended Data Fig. 1e). This wood was brought for analysis to the Forest Products Research and Development Institute of the University of the Philippines Los Baños. It was positively identified as *Diospyros* sp. of the family Ebenaceae based on parenchyma cells shape in transverse, tangential and radial sections. This genus groups plants ranging from small shrubs to large trees. The majority of the species of the genus *Diospyros* are native to the tropics but are now rarely found in the low-altitude forests in the Philippines. Six species are presently found in the Cagayan Valley with habitat ranging from low-medium elevation primary forests to low-medium elevation limestone and dipterocarp forests[51].

Five sediment samples of approximately 100g each were taken for palynological analysis from Unit F in the excavation profile NE/East. All the samples were taken from freshly scraped stratigraphic profiles, sampling from bottom to top with 10cm interval using a repeatedly cleaned trowel. The samples were treated and processed with the protocol described by Sémah[52] at the palynology laboratory of the Institut de Recherche pour le Développement (IRD) in Bondy, France. The sediments were found to be barren of any pollen.

The absence of any pollen and the presence of a waterlogged wood fragment in the clayey Unit F dating back to between 731±31 and 706±70 ka is consistent with the interpretation on the deposition process of Unit F as a mudflow consecutive to a volcanic eruption. The presence of volcanic ash in the mudflow Unit F would have indeed both favoured the preservation of organic fragments such as wood and prevented the preservation of pollen.

Faunal analysis

Along with the partial *Rhinoceros philippinensis* fossil skeleton (Extended Data Figure 2a), Unit F contained other vertebrate fossils concentrated near the base. This fauna is briefly described here and compared to older surface findings to better outline the now extinct Middle Pleistocene fauna of The Philippines.

An intermediate *Stegodon* molar fragment (II-2014-J1-437) has two slightly worn ridges preserved, both bearing five apical mammillae (Extended Data Figure 2e). The smooth lateral surfaces and heavy cement suggests it represents an upper or lower m1, m2 or m3. Van den Bergh (1999: 58)[53] noted that a limited number of mamillae, between 4 and 7 per ridge, is a plesiomorphic trait. In the contemporary fauna from Java, *Stegodon trigonocephalus*, individual ridges have 9 to 15 mammillae. The maximum width of the largest ridge of the Kalinga specimen is 55 mm, its corresponding mesiodistal length is 18.8 mm and its height is 40.5 mm. These measurements are only indicative considering the unknown serial number of the molar. In von Koenigswald[54] and de Vos and Bautista[55], description of the surface megafaunal remains from The Philippines, only one species of *Stegodon* is recognized for the archipelago namely *Stegodon luzonensis*, as proposed by von Koenigswald in 1956. The dimensions and number of mammillae of the specimen from Kalinga fit within the variability of these specimens (width of lower m3 (NMP-593) = 59 mm; unworn height = 41 mm) and is therefore here attributed to *Stegodon* cf. *luzonensis*.

A complete second right upper molar (II-2014-J1-344), four upper molar fragments (II-2014-J1-345, II-2014-J1-346, II-2014-J1-347, and II-2014-J1-577) and a proximal fragment of a left radius (II-2014-J1-488), all of Cervidae were recovered (Extended Data Figure 2c,d). The complete second right upper molar is unworn and shows an intact entostyle and bucco-lingually compressed mesial and distal fossa, both of which features are comparable to what is seen in *Cervus*. The parastyle further presents a distal cleft comparable to what is found in *Cervus mariannus*. The length of the upper second molar is 17.3 mm, its mesial width is 18.5 mm and its distal width is 18.1 mm. These dimensions are within the range of *Cervus mariannus* (length range: 15.1-18.3 mm, mesial width range: 15.8-18.7 mm, distal width range: 15.3-18.7 mm), and appear larger than the two other species presently known from The Philippines: *Cervus alfredi* (length range: 13.5-17.3 mm, mesial width range: 15-15.7 mm, distal width range: 14.1-15.5 mm) and *Axis calamianensis* (length range: 13.3-17.8 mm, mesial width range: 11.5-12.7 mm, distal width range: 11.8-13.3 mm). Furthermore, these dimensions are larger than other extant and fossil Cervidae species from Southeast Asia, including *Muntiacus muntjak*, *Axis lydekkeri*, *Axis lydekkeri ngebuensis*, and smaller than the dimensions of *Cervus unicolor*[56].

Although there have been several claims for Pleistocene Cervid fossils in The Philippines, the literature does not provide enough detail regarding the findings, nor does the literature include a morphological description or geological provenance, as noted by de Vos and Bautista[55]. Currently, only fragments of antlers are present in the collections of the National Museum of The Philippines from surface discoveries. De Vos and Bautista[55] conclude that, based on the size of these museum fragments, they pertain to a small Cervid, presumably *Axis*. Our observations are that we can quite confidently

attribute the Cervidae material from Kalinga to the Philippine brown deer *Cervus mariannus*, which is presently the only known species from Luzon Island. It therefore appears that this species, endemic to The Philippines, was already present in the archipelago at least 650,000 years ago.

A varanid fibula (II-2014-J1-350) and a femur fragment (II-2014-J1-351) were recovered from Unit F (Extended Data Figure 2b). Both the fibula and the femur have three-quarters of the distal portion of the shaft preserved. The *Varanus salvator* complex has been recently split into eight to eleven species based on colour and scales number[57]. Of these, three species have been described from Luzon Island, *Varanus marmoratus*, *Varanus olivaceus* and the recently newly discovered species from the Sierra Madre, *Varanus bitatawa*[58]. The morphology of the two bones from the Kalinga site is simple and their general shape is similar to the one of the monitor lizard complex, *Varanus salvator*[59], without any possible distinction between the different species. The dimensions of the fibula (maximum width: 10.9 mm) and the femur (maximum width: 19.2 mm) are slightly smaller than that of modern adult monitor lizard dimensions (fibula maximum width range: 11.89-15.46 mm and femur maximum width range: 16.30-21.41 mm). If our varanid fossil bones are of a monitor lizard, they constitute the oldest of this species complex ever recovered from The Philippines. In addition to these varanid fossils, other reptilian fossils excavated from Unit F comprise carapace fragments of Geoemydidae (Extended Data Figure 9).

The Kalinga site has a clear endemic unbalanced fauna where carnivores are absent which is typical of islands from all around the world (Extended Data Fig. 9). Furthermore, this faunal composition of Luzon during the Pleistocene is biased in favour of taxa with overseas dispersal abilities, including proboscideans, deer and pigs, while most other mainland taxa are missing.

Bone modifications

All the bones were examined under low magnification using a DinoLite digital microscope. The bones with surface modifications were then examined under a light microscope under different magnifications and photographs were taken. Additionally, the surface of some of the bones were casted using a Provil Novo light regular silicon, and the epoxy resin replicas were digitized using an Alicona InfiniteFocus, which was preferred to scanning electron microscopy for its better resolution and precision. Identification and description of anthropogenic marks were made following the combination of criteria listed by Dominguez-Rodrigo and co-authors[60].

Within the faunal assemblage excavated from Kalinga Unit F, 13 of the *Rhinoceros philippinensis* fossils show clear marks of hominin activity. One percussion mark was observed on each of the humeri (Fig. 3a,c), in both opposite elements characterized by large conchoidal scar typical of direct percussion on a bone surface with a stone usually made with the aim to reach the marrow[61]. One of these impacts further produced a bone flake that is still adhering to the right humerus, which is further evidence of the anthropogenic origin of this bone surface modification as demonstrated through experiments[61]. A total of 27 cut marks were confidently identified on 11 of the rhinoceros fossil bones (one metacarpal and ten ribs). On the contrary, four ribs presented evidence for abrasion by sediment and/or trampling, while no

carnivore marks could be identified on any of the bones. All the groves we identified as anthropogenic marks – whether they are on the metacarpal or on the ribs – exhibit five out of six diagnostic criteria for butchery marks as listed by Dominguez-Rodrigo and co-authors[60], such as V-shape cross-sections, hertzian cones, asymmetrical profiles, barbs and shoulder effects. Not observed with high confidence were microstriations in the bottom of the grooves which are nevertheless rarely preserved on archaeological material[60] (Fig. 3). Of the anthropogenic marks, four cut marks were observed on the right metacarpal IV and 23 cut marks were observed on 10 ribs. Of the latters, seven were located on a ventral surface, 12 were on a lateral surface, two were on an anterior and two on posterior surfaces of ribs. Seven cut marks were positioned close to the proximal extremity of ribs and six were close to the distal extremity of ribs. All those marks are oriented transversely to the long axis of the ribs.

While cut marks have a mean length of 8.7 mm and a width of 0.4 mm, abrasion striations are shorter and narrower (mean length is 3.3 mm and mean width is 0.2 mm). The abrasion marks on the rhinoceros bones are also more superficial than the anthropogenic cut marks. Furthermore, while cut-marked bones had one to a maximum of four larger parallel groves on either surface, the abrasion striations on bones were multiple and multidirectional (Fig. 3c2). The abrasion marks were located on the ventral surfaces of two ribs, on the lateral surface of one rib and on the anterior surface of another rib.

Taking into account the presence of clear percussion marks, the criteria recently defined By Dominguez-Rodrigo and co-authors[60] for the recognition of cut marks, the special position of the marks on the fossil rhinoceros skeleton and on the individual bones, and considering the shape and size of the other groove marks apparently caused by abrasion by the sediments, the presence of cut marks would appear evident. Several studies have recorded higher frequencies of V-grooves in cut marks as compared to striations caused by trampling or sediment abrasion, which are non-organized. Berhensmeyer[62] noted that isolated marks can be misinterpreted as cut marks, but that multiple organized marks, positioned on specific areas such as metapodials[63], can be confidently attributed to cut marks. In addition, Crader[64] observed a higher frequency of cut marks on the ribs of single-carcass bone scatters of butchered elephants rather than on other skeletal elements. Therefore, the location of the cut marks on the Kalinga rhinoceros skeleton support their identification as such, and this evidence supports the conclusion that the rhinoceros carcass had been subjected to butchery activity by hominins.

Lithic technology

The lithic assemblage has been produced from siliceous and igneous rocks by means of various knapping aptitudes and record clear technical attributes (butt, percussion cones)[65]. The knapping techniques include the use of direct hard hammer stone percussion, both bipolar and tangential, and this is also evidenced by crush marks on the distal extremity of two dacitic pebbles. The knapping strategies are oriented towards short and non-organized reduction sequences, resulting in non-standardized flake morphologies and dimensions, and without any intentional retouch usually referred to as expedient

technology. The flakes are sometimes elongated and trapezoid, sometimes short, triangular and canted (*déjeté*). All six cores have a residual cortex with at least two short debitage phases (maximum three removals) with bipolar and linear removal directions. The striking platforms are always built on the previous negatives or fracture plans. The knapping angles are uniformly close to 90°, and the negative flake scars show both a bulb resulting from direct freehand percussion and its counter shock resulting from the use of an anvil. The lithic industry excavated in Kalinga is therefore diverse in its techniques and final products.

A diversity of the artefacts is characteristic of the Southeast Asian lower Palaeolithic which is broadly defined as Acheulean (mode 2) for its large cutting tools such as handaxes but which is also frequently composed of smaller, often unretouched flakes[66]. While they have been found primarily outside clear stratigraphic context[67], the Javanese horsehooves, bolas and polyhedrons, along with handaxes and the small 'Sangiran flakes' were recovered in a well-dated 800 ka old layer[68] at Ngebung 2 site of the Sangiran Dome[69,70]. This assemblage of stone tools is associated with faunal remains – some intentionally broken – that can be attributed to the Trinil H.K. fauna[71], and with a *Homo erectus* molar[72]. Further to the East, In the So'a Basin of Flores Island, mostly unretouched small flakes (2 to 4 cm) are dated to one million years[73]. These artefacts, produced through percussion on anvil, are described as similar to the 700 ka old flakes recovered on the same island and associated with a *Homo floresiensis*-like hominin at the So'a Basin site of Mata Menge[74]. Similarly, small unretouched flakes produced by anvil percussion have also been recovered from the Kalinga site, and are of the same age.

It is also noteworthy that, as in Kalinga site, lithic artefacts associated with tektites have been recovered to the north of the Philippines in the Bose Basin in China[75]. These artefacts are typical Acheulean (mode 2) tools including handaxes.

Although not found in stratigraphic context, Acheulean (mode 2) industry is also present in the Philippines at the Arubo 1 site[76]. This assemblage has been assumed to be lower Palaeolithic, and contains a handaxe, and what Pawlik[77] interprets as a horsehoof-like core and a "quasi-Levallois" flake, all of which were found eroding from the present day soil[78]. A total of fifteen tools were identifiable unifacial and bifacial cores and flakes out of 197 lithic artefacts. A further handaxe, likewise not recovered from a clear stratigraphic context, was found by V.J. Paz in the Dewil Valley on Palawan Island (as cited by Dizon and Pawlik[79]). Peterson[80] re-studied the likewise undated Novaliches dam area stone artefacts found in the 1930's by Otley H. Beyer in North Manila and considered them as similar to the Bacsonian and Hoabinhian industries which are both younger than the Kalinga site. The so-far oldest prehistoric site of the Philippine archipelago, the Callao Cave, where a 67 ka old hominin third metatarsal was also discovered, has delivered no lithic artefacts but some cut marks identified on some of the cervid bones that originate from the same sedimentary breccia layer although they are seemingly younger[81].

Due to a tendency for a lack of constrained dating of artefacts recovered from regional context, only limited comparisons of the well-dated Kalinga lithic material can be made. We note, however, the

predominance of unifacial technology in Island Southeast Asia, the recurrence of anvil percussion and the production of small unretouched flakes along with larger implements. In comparison to the well-published Arubo 1 site, large cutting tools account for a small proportion of the assemblage, which is furthermore mostly composed of shatter fragments (182 pieces out of 197 artefacts). Shatter fragments showing some characteristic features have been described in Liang Bua as common byproducts of percussion on anvil[82]. More insights on the shatter fragments from Arubo 1 would therefore certainly better highlight similarities and dissimilarities with the Kalinga material in which percussion on anvil has been positively identified.

Stone artefacts associated with very large game butchery in Lower Palaeolithic sites like in Kalinga are generally small-sized. Experiments have demonstrated that a small number of simple flakes is sufficient to butcher a very large carcass, such as an elephant[83,84]. Most archaeological sites that have yielded a single carcass of a very large game animal, whether in Africa or Europe, have a limited number of stone tools, and, as noted by Isaac[85] and more recently by Delagnes and co-authors[86], typically less than one hundred pieces. For example, this is the case at Fuente Nueva 3 with 17 flakes[87], Castel di Guido with 96 flakes[88], La Polledrara with 61 artefacts[89], Notarchirico with 42 chert and limestone artefacts[90], Southfleet Road with about a hundred artefacts[91], 14 flint and quartzite artefacts from Ambrona[92] and 34 flint and quartzite artefacts from Aridos 2[93]. Only a few Lower to early Middle Pleistocene sites including evidence of very large game butchery have delivered more than a hundred artefacts: Koobi Fora's FxJj 3 site (also named Hippopotamus/artefact site or HAS) with 122 recovered stone-tools[85], Barranc de la Boella - Pit 1 with 125 recovered lithic artefacts[94], Aridos 1 with 331 recovered artefacts[93] and Ficoncella with 409 lithic implements of which 296 represent small flakes[95]. The same observations are true for more recent sites dating back to the late Middle Pleistocene[96]. Our findings at the Kalinga site are overall coherent with these observations: the number of lithic implements directly associated with the rhinoceros carcass is limited, less than a hundred pieces, the raw materials are varied and most of the flakes are small and unretouched.

Supplementary Table 1 | ESR results obtained on quartz extracted from sediments. Analytical uncertainties and ages are given with ±1σ. Water contents (%) were estimated by the difference in mass between the natural sample and the same sample dried for a week in an oven at 50°C. Dose rates were determined using dose rate conversion factor updated by Guerin and co-authors[25]. Alpha and beta attenuations were estimated for the selected grain sizes from the tables of Brennan[103]; k-value of 0.15 [7], cosmic dose rate calculated from the equations of Prescott & Hutton[30]. We have at present no means to know precisely when the erosion took place and since when the archaeological material became buried under less than 7m of sediment. Therefore, a depth of 2.60m, which is the thickness between the base of layer A4 and the top of layer G1 still covering Unit A and F where the sample was taken, was used for the cosmic dose rate estimation of Unit A. A depth of 3.40m was used for the cosmic dose rate estimation of Unit G which corresponds to the thickness measured between the base of layer G1 and the laminated silty layer J4 considering that part of Unit J still covers Unit G where the sample was taken. A cosmic dose estimated from a depth of 7m would increase the age for the Unit A by 13% and by 16% for Unit G. The bleaching rate δ_{bl} (%) is determined by comparison of the ESR intensities of the natural and bleached aliquotes ($\delta_{bl}= ((I_{nat}-I_{bl})/I_{nat})x100$). Mean age are weighted average calculation using Isoplot software.

	D_α (µGy/a)	D_β (µGy/a)	D_γ + cosmic (µGy/a)	Dγ (µGy/a)	D cosmic (µGy/a)	D_a (µGy/a)	Water %	δ_{bl} %	D_E (Gy)	Age (ka)	Mean age (ka± 1σ)
Unit A -Al	7 ± 1	189±12	220±11	86±9	134±6	416±16	15	100	303±10	728±28	727±30
Unit A -Ti	7 ± 1	189±12	220±11	86±9	134±6	416±16	15	100	305±11	733±32	
Unit G -Al	9 ± 1	224±13	195±10	47±6	148±8	428±17	13	100	293±20	685±49	701±70
Unit G -Ti	9 ± 1	224±13	195±10	47±6	148±8	428±17	13	100	306±21	717±50	

Supplementary Table 2 | Radioelements content of the different Kalinga sedimentary units measured by ESR. $^{226}Ra/^{238}U$ and $^{222}Rn/^{238}U$ are activity ratios.

	^{238}U (ppm)	^{232}Th (ppm)	^{40}K (%)	$^{226}Ra/^{238}U$	$^{222}Rn/^{238}U$
Unit A	0,270 ± 0,054	1,059 ± 0,074	0,272 ± 0,009	1,010 ± 0,137	0,944 ± 0,056
Unit F [1]	1,852 ± 0,121	3,154 ± 0,144	1,899 ± 0,026	1,035 ± 0,200	0,869 ± 0,093
Unit G	0,277 ± 0,049	0,894 ± 0,063	0,222 ± 0,008	0,931 ± 0,127	0,887 ± 0,051

[1] Mean values from three sediment samples

Supplementary Table 3 | $^{40}Ar/^{39}Ar$ individual age obtained on large transparent plagioclase crystals (1-1.5mm) for each units investigated.

Lab. code	^{40}Ar (moles)	^{36}Ar V	±σ36 V	^{37}Ar V	±σ37 V	^{38}Ar V	±σ38 V	^{39}Ar V	±σ39 V	^{40}Ar V	±σ40 V	D[(1)]	±%2 σ_D	%^{40}Ar*	Age (Ka)	±σ	K/Ca	± 1σ
UNIT A																		
N1440-01	4.469 E-16	1.161 E-06	3.028	0.0007286	1.167	0.0000003	5.195	3.368 E-05	0.945	3.262 E-04	0.301	1.01117	0.1	18.86	1110.6	± 192.7	0.0077	± 0.0001
N1440-02	6.957 E-16	1.862 E-06	0.830	0.0010018	0.671	0.0000010	3.362	3.810 E-05	0.528	5.078 E-04	0.148	1.01122	0.1	12.73	1036.3	± 81.9	0.0063	± 0.0001
N1440-03	3.029 E-16	8.823 E-07	1.251	0.0009109	1.000	0.0000007	3.404	3.618 E-05	0.412	2.211 E-04	0.347	1.01114	0.1	27.23	1014.7	± 62.5	0.0066	± 0.0001
N1440-04	2.204 E-16	6.547 E-07	1.171	0.0007606	0.721	0.0000006	3.373	2.861 E-05	0.347	1.608 E-04	0.432	1.01114	0.1	31.70	1088.2	± 56.0	0.0063	± 0.0001
N1440-05	2.030 E-16	5.466 E-07	0.724	0.0005167	0.722	0.0000005	4.152	2.474 E-05	0.134	1.482 E-04	0.468	1.01113	0.1	29.12	1060.1	± 38.7	0.0080	± 0.0001
N1440-06	1.268 E-16	3.406 E-07	5.007	0.0003089	0.925	0.0000002	6.634	1.429 E-05	1.323	9.253 E-05	0.614	1.01111	0.1	27.67	1089.6	± 219.6	0.0077	± 0.0001
N1440-07	1.557 E-16	4.503 E-07	1.994	0.0006225	0.781	0.0000005	4.051	2.953 E-05	0.670	1.136 E-04	0.675	1.01112	0.1	43.34	1013.7	± 60.5	0.0079	± 0.0001
UNIT G																		
N1438-01	2.477 E-16	8.033 E-07	2.644	0.0017906	0.827	0.0000016	2.194	8.396 E-05	0.445	1.808 E-04	0.740	1.01114	0.1	78.82	1053.8	± 51.5	0.0078	± 0.0001
N1438-02	1.629 E-15	4.102 E-06	0.783	0.0005999	0.675	0.0000011	2.216	2.287 E-05	1.007	1.189 E-03	0.195	1.01141	0.1	2.69	872.6	± 292.7	0.0063	± 0.0001
N1438-03	4.261 E-16	1.339 E-06	1.085	0.0017111	0.773	0.0000011	2.867	6.298 E-05	0.509	3.111 E-04	0.334	1.01117	0.1	33.36	1028.0	± 50.5	0.0061	± 0.0001
N1438-04	3.685 E-16	1.269 E-06	2.244	0.0021880	0.688	0.0000015	2.582	8.559 E-05	0.555	2.690 E-04	0.350	1.01117	0.1	50.64	991.3	± 65.8	0.0065	± 0.0001
N1438-05	1.853 E-16	5.135 E-07	2.342	0.0004342	0.770	0.0000004	4.186	1.723 E-05	1.020	1.353 E-04	0.665	1.01113	0.1	22.78	1113.9	± 136.6	0.0066	± 0.0001
N1438-06	1.374 E-16	5.063 E-07	3.076	0.0009813	0.786	0.0000007	6.187	4.016 E-05	0.819	1.003 E-04	0.684	1.01111	0.1	59.43	924.1	± 76.1	0.0068	± 0.0001
N1438-07	4.927 E-16	1.343 E-06	0.686	0.0008393	0.766	0.0000006	4.860	3.495 E-05	0.525	3.596 E-04	0.260	1.01118	0.1	14.81	947.9	± 59.0	0.0069	± 0.0001
N1438-08	2.684 E-16	7.181 E-07	4.124	0.0006374	0.768	0.0000005	3.405	2.751 E-05	1.135	1.959 E-04	0.592	1.01114	0.1	27.18	1203.9	± 203.2	0.0072	± 0.0001

Supplementary Table 4 | $^{40}Ar/^{39}Ar$ background corrections.

Lab. Code	^{36}Ar	±σ36	^{37}Ar	±σ37	^{38}Ar	±σ38	^{39}Ar	±σ39	^{40}Ar	±σ40
	V	V	V	V	V	V	V	V	V	V
					UNIT A					
N1440-01	1.689E-07	7.430E-09	1.348E-08	6.848E-09	2.819E-08	1.381E-08	1.278E-07	1.265E-07	3.752E-05	4.502E-07
N1440-02	1.689E-07	7.430E-09	1.348E-08	6.848E-09	2.819E-08	1.381E-08	1.278E-07	1.265E-07	3.752E-05	4.502E-07
N1440-03	1.689E-07	7.430E-09	1.348E-08	6.848E-09	2.819E-08	1.381E-08	1.278E-07	1.265E-07	3.752E-05	4.502E-07
N1440-04	1.704E-07	1.687E-09	2.668E-08	4.376E-09	7.665E-08	1.134E-08	7.640E-08	9.932E-09	3.637E-05	3.637E-07
N1440-05	1.704E-07	1.687E-09	2.668E-08	4.376E-09	7.665E-08	1.134E-08	7.640E-08	9.932E-09	3.637E-05	3.637E-07
N1440-06	1.704E-07	1.687E-09	2.668E-08	4.376E-09	7.665E-08	1.134E-08	7.640E-08	9.932E-09	3.637E-05	3.637E-07
N1440-07	1.704E-07	1.687E-09	2.668E-08	4.376E-09	7.665E-08	1.134E-08	7.640E-08	9.932E-09	3.637E-05	3.637E-07
					UNIT G					
N1438-01	2.374E-07	8.451E-09	1.100E-08	1.099E-08	4.761E-08	1.409E-08	2.128E-06	1.609E-07	5.169E-05	6.203E-07
N1438-02	2.374E-07	8.451E-09	1.100E-08	1.099E-08	4.761E-08	1.409E-08	2.128E-06	1.609E-07	5.169E-05	6.203E-07
N1438-03	2.400E-07	9.456E-09	4.211E-08	1.049E-08	3.247E-08	7.501E-09	8.900E-07	9.345E-08	4.515E-05	6.411E-07
N1438-04	2.400E-07	9.456E-09	4.211E-08	1.049E-08	3.247E-08	7.501E-09	8.900E-07	9.345E-08	4.515E-05	6.411E-07
N1438-05	2.400E-07	9.456E-09	4.211E-08	1.049E-08	3.247E-08	7.501E-09	8.900E-07	9.345E-08	4.515E-05	6.411E-07
N1438-06	1.445E-07	5.347E-09	1.750E-08	5.565E-09	1.046E-08	7.008E-09	7.160E-08	5.513E-08	3.088E-05	3.705E-07
N1438-07	1.445E-07	5.347E-09	1.750E-08	5.565E-09	1.046E-08	7.008E-09	7.160E-08	5.513E-08	3.088E-05	3.705E-07
N1438-08	1.088E-07	7.398E-09	1.100E-08	1.099E-08	4.364E-08	6.895E-09	7.173E-08	7.166E-08	2.445E-05	3.619E-07

Supplementary Table 5 | Magnetic intensities and Characteristics Remanent Magnetization directions before and after demagnetization.

No	Specimen	Intensity (A/m)		Remanence direction (ChRMs)	
		Before demagnetization	After demagnetization	Mean declination	Mean Inclination
1	HT-1A (AF)	35.93 E -03	2.595 E -03	353.4	22.6
2	HT-1B (AF)	62.48 E -03	5.736 E -03	356.6	20.2
3	HT-1C (AF)	71.24 E -03	5.081 E -03	356.3	32.2
4	HT-1D (AF)	47.90 E -03	4.327 E -03	348.2	27.2
5	HT-1K (AF)	72.78 E -03	4.250 E -03	356.8	27.1
6	HT-1E (TD)	36.95 E -03	2.723 E-03	343.8	23

References

1 Ingicco, T., van den Bergh, G., de Vos, J., Castro, A., Amano, N., Bautista, A. A new species of *Celebochoerus* (Suidae, Mammalia) from the Philippines and the paleobiogeography of the genus *Celebochoerus* Hooijer, 1948. *Geobios* 49:285-291 (2016)

2 Mathisen, M. & Vondra, C. The fluvial and pyroclastic deposits of the Cagayan Basin, northern Luzon, Philippines—An example of non-marine volcaniclastic sedimentation in an interarc basin. *Sedimentology* 30, 369-392 (1983).

3 Mathisen, M. E. *Plio-Pleistocene geology of the Central Cagayan Valley, Northern Luzon, Philippines* PhD thesis, Iowa State University, (1981).

4 Millot, G. *Geology of Clays, Weathering, Sedimentology, Geochemistry*. Springer-Verlag Berlin Heidelberg 430p. (1970)

5 Baldermann, A., Dohrmann, R., Kaufhold, S., Dietzel, M. The Fe-Mg-saponite solid solution series - A hydrothermal synthesis study. *Clay Minerals* 49(3):391-415 (2014)

6 McDougal, I. & Harrison, M. Geochronology and thermochronology by the $^{40}Ar/^{39}Ar$ method. Oxford University Press. 269p. (1999)

7 Yokoyama, Y., Falguères, C., Quaegebeur, J.P. ESR dating of quartz from Quaternary sediments: first attempt. *Nuclear tracks* 10:921–928. (1985)

8 Bahain J.-J, Falguères C., Dolo J.-M., Antoine P, Auguste P., Limondin-Lozouet N., Locht J.-L., Tuffreau A. ESR/U-series dating of teeth recovered from well-stratigraphically age-controlled sequences from Northern France. *Quaternary Geochronology* 5:371-375 (2010)

9 Duval, M. Grün, R. Are published ESR dose assessments on fossil tooth enamel reliable? *Quaternary Geochronology* 31:19-27 (2016)

10 Shao, Q., Bahain, J.-J., Falguères, C., Peretto, C., Arzarello, M., Minelli, A., Hohenstein, U.T., Dolo, J.-M., Garcia, T., Frank, N., Douville, E. New ESR/U-series data for the early middle Pleistocene site of Isernia la Pineta, Italy. *Radiation Measurements* 46:847-852. (2011)

11 Hiess, J., Condon, D.J., McLean, N., Noble, S.R. $^{238}U/^{235}U$ systematics in terrestrial uranium-bearing minerals. *Science* 335:1610-1614 (2012)

12 Cheng, H., Edwards, R.L., Shen, C.-C., Polyak, V.J., Asmerom, Y., Woodhead, J., Hellstrom, J., Wang, Y., Kong, X., Spötl C., Wang, X., Alexander Jr., E.C. Improvements in ^{230}Th dating, ^{230}Th and ^{234}U half-life values, and U–Th isotopic measurements by multi-collector inductively coupled plasma mass spectroscopy. *Earth and Planetary Science Letters* 371–372:82–91 (2013)

13 Shao, Q., Chadam, J., Grün, R., Falguères, F., Dolo, J-M., Bahain, J-J. The mathematical basis for the US-ESR dating method. *Quaternary Geochronology* 30(A): 1-8. (2015)

14 Grün, R., Schwarcz, H.P., Chadam, J.M. ESR dating of tooth enamel: coupled correction for U-uptake and U-series disequilibrium. *Nuclear Tracks and Radiation Measurements* 14:237-241 (1988)

15 Ikeya M. *New applications of Electron Spin Resonance*. World Scientific publishing, Singapore. (1993)

16 Weil, J.A., 1984. A review of electron Spin Spectroscopy and its applications to the study of paramagnetic defects in crystalline quartz. *Physics and Chemistry of Minerals*, 10:149-165. (1984)

17 Falguères C., Yokoyama Y. & Miallier D. Stability of some centres in quartz. *Nuclear Tracks Radiation Measurements* 18:155-161 (1991)

18 Voinchet, P., Bahain, J.-J., Falguères, C., Laurent, M., Dolo, J.-M., Despriée, J., Gageonnet R. ESR dating of quartz extracted from Quaternary sediments: Application to fluvial terraces system of Northern France. *Quaternaire* 15:135-141. (2004)

19 Toyoda, S., Falguères C. The method to represent the ESR signal intensity of the aluminium hole center in quartz for the purpose of dating. *Advances in ESR applications* 20:7-10. (2003)

20 Duval M. and Guilarte V. ESR dosimetry of optically bleached quartz grains extracted from Plio-quaternary sediment: evaluating some key aspects of the ESR signal associated to the Ti-center. *Radiation Measurement*s 78:28–41 (2015)

21 Duval M, Grün R, Falguères C, Bahain JJ, Dolo JM. ESR dating of Lower Pleistocene fossil teeth: Limits of the single saturating exponential (SSE) function for the equivalent dose determination. *Radiation Measurements* 44:477-48 (2009)

22 Voinchet P., Yin G., Falguères C., Liu C., Han F., Sun X., Bahain J.-J. ESR dose response of Al center measured in quartz samples from the Yellow River (China): Implications for the dating of Upper Pleistocene sediment. *Geochronometria* 40(4):341-347 (2013)

23 Mercier N., Falguères C. Field gamma dose-rate measurement with a NaI (Tl) detector: re-evaluation of the "threshold" technique. *Ancient TL* 25:1-4 (2007)

24 Yokoyama Y, Nguyen HV (1980) Direct and non-destructive dating of marine sediments, manganese nodules and corals by high resolution gamma-ray spectrometry. *In: Goldberg ED, Horibe Y, Saruhashi K (eds) Isotope Marine Chemistry*, Uchida Rokakuho, Tokyo, pp 259-289 (1980)

25 Guérin, G., Mercier, N. Adamiec, G. Dose-rate conversion factors: update. *Ancient TL* 29:5–8 (2011)

26 Laurent, M., Falguères C., Bahain, J.J., Rousseau, L., Van Vliet-Lanoë B. ESR dating of quartz extracted from Quaternary and Neogene sediments: method, potential and actual limits. *Quaternary Science Reviews* 17:1057-1061. (1998)

27 Brennan, B. J. Beta doses to spherical grains. *Radiation Measurements* 37:299-230 (2003)

28 Brennan B, Lyons R, Phillips S. Attenuation of alpha particle track dose for spherical grains. Nuclear tracks *Radiation Measurements* 18(1/2):249-253 (1991)

29 Grün, R. A cautionary note: use of the "water content" and "depth for cosmic ray dose rate" in AGE and DATA programs'. *Ancient TL* 12:50-51 (1994)

30 Prescott, J.R., Hutton, J. T., 1994. Cosmic ray contributions to dose rates for Luminescence and ESR Dating: Large depths and long-term time. *Radiation Measurements* 23:497-500 (2011)

31 Dingman SL. *Physical hydrology*. 3rd edition. Waveland Press. Long Grove. 643p. (2014)

32 Murray AS, Roberts RG. Determining the burial time of single grains of quartz using optically stimulated luminescence. *Earth and Planetary Science Letters* 152:163-180 (1997)

33 Vandenberghe D, De Corte F, Buylaert JP, Kucera J, Van den haute P. On the internal radioactivity in quartz. *Radiation Measurements* 43:771-775 (2008)

34 Ludwig, K.R., 2003, *User's Manual for Isoplot/Ex, Version 3.0*, A geochronological toolkit for Microsoft Excel Berkeley Geochronology Center. Special Publication, v. 4, Berkeley Geochronology Center, 2455 Ridge Road, Berkeley, CA 94709, USA. (2003)

35 Nomade, S., Gauthier, A., Guillou, H., Pastre, J.F $^{40}Ar/^{39}Ar$ temporal framework for the Alleret maar lacustrine sequence (French Massif Central): Volcanological and Paleoclimatic implications. *Quaternary Geochronology* 5:20-27. (2010)

36 Nomade, S., Renne, P.R., Vogel, N., Deino, A.L., Sharp, W.D., Becker, T.A., Jaouni, A.R., Mundil, R. Alder Creek sanidine (ACs-2), A Quaternary $^{40}Ar/^{39}Ar$ dating standard tied to the Cobb Mountain geomagnetic event. *Chemical Geology* 218:315–338. (2005)

37 Niespolo, E.M., Rutte, D., Deino, A., Renne, P.R. Intercalibration and age of the Alder Creek sanidine 40Ar/39Ar standard. *Quaternary Geochronology* (In press)

38 Min, K.W., Mundil, R., Renne, P.R., Ludwig, K.R. A test for systematic errors in $^{40}Ar/^{39}Ar$ geochronology through comparison with U/Pb analysis of a 1.1-Ga rhyolite. *Geochimica Cosmochimica Acta* 64:73-98. (2000)

39 Lee, J.Y., Marti, K., Severinghaus, J.P., Kawamura, K., Yoo, H.S. Lee, J.B., Kim, J.S. A redetermination of the isotopic abundances of atmospheric Ar. *Geochimica et Cosmochimica Acta* 70:4507-4512. (2006)

40 Ludwig, K.R. Isoplot 3.0-a Geochronological Toolkit for Microsoft Excel. *In Special Publication No. 4. Berkeley Geochronology Center*: Berkeley, CA. (2001)

41 Lurcock, P.C. and Wilson, G. S. PuffinPlot: A versatile, user-friendly program for palaeomagnetic analysis. *Geochemistry, Geophysics, Geosystem* 13:1-6 (2012)

42 Kirschvink, J. The least-squares line and plane and the analysis of palaeomagnetic data. *Geophysical Journal International* 62, 699-718 (1980)

43 Fisher, R. Dispersion on a sphere. *Proceedings of the Royal Society London*, Series A 217:295–305 (1953)

44 Butler, R. F. *Paleomagnetism: Magnetic Domains to Geologic Terrains*. Blackwell Scientific Publications, (1992)

45 Mark, D.F., Renne, P.R., Dymock, R.C., Smith, V.C., Simon, J.L., Morgan, L.E., Staff, R.A., Ellis, B.S., Pearce, N.J.G. High-precision $^{40}Ar/^{39}Ar$ dating of pleistocene tuffs and temporal anchoring of the Matuyama-Brunhes boundary. *Quaternary Geochronology* 39:1-23 (2017)

46 Neri, L.A.M. Philippine obsidian and its archaeological implications. *Bulletin of the Indo-Pacific Prehistory Association* 27:154-162 (2007)

47 Werner, T. and Borradaile, G.J. Homogeneous magnetic susceptibilities of tektites: Implications for extreme homogenization of source material. *Physics of the Earth and Planetary Interiors* 108:235-243 (1998)

48 Rochette, P., Gattacceca, J., Devouard, B., Moustard, F., Bezaeva, N.S., Cournède, C., Scaillet, B. Magnetic properties of tektites and other related impact glasses. *Earth and Planetary Science Letters* 432:381-390 (2015)

49 Frahm, E., and Feinberg, J.M. From flow to quarry: Magnetic properties of obsidian and changing the scales of archaeological sourcing. *Journal of Archaeological Science* 40:3706-3721 (2013)

50 Koeberl, C. The geochemistry of tektites: an overview. *Tectonophysics* 171:405-422 (1990)

51 LaFrankie, J.V. *Trees of Tropical Asia: an illustrated guide to diversity*. Philippines: Black Tree Publishing. (2010)

52 Sémah, A-M. *Le Milieu naturel lors du premier peuplement de Java, Résultats de l'analyse pollinique*. Unpublished PhD Thesis, Université de Provence, 188p. 3 volumes (1986)

53 van den Bergh, G.D., 1999. The Late Neogene elephantoid-bearing faunas of Indonesia and their palaeozoogeographic implications. Scripta Geologica 117, 430.

54 Von Koenigswald, G.H.R., Fossil Mammals from the Philippines. Natl. Res. Counc. Philipp. Pap. 22 Proc. Fourth Far-East. Prehistory Congr. 1–14 (1956)

55 De Vos J. and Bautista A. Preliminary notes on the vertebrate fossils from the Philippines. Proceedings of the Society of Philippine Archaeologists 1, 46–62 (2003)

56 Moigne, A.M., Due Awe, R., Sémah, F., Sémah, A.M. The cervids from the Ngebung site (Kabuh series, Sangiran Dome, Central Java) and their biostratigraphical significance. *Modern Quaternary Research in Southeast Asia*, 18:31-44 (2004)

57 Welton, L.J., Siler, C.D., Oaks, J.R., Diesmos, A.C., Brown, R.M. Multilocus phylogeny and Bayesian estimates of species boundaries reveal hidden evolutionary relationships and cryptic diversity in Southeast Asian monitor lizards. *Molecular Ecology* 22(13): 3495-3510 (2013)

58 Welton L.J., Siler C.D., Bennet D., Diesmos, A., Roy Duya, M., Dugay, R., Rico, E.L.B., van Weerd, M., Brown, R.M. A spectacular new Philippine monitor lizard reveals a hidden biogeographic boundary and a novel flagship species for conservation. *Biology Letters*, 6, 654–658 (2010)

59 Auffenberg, W. *Gray's Monitor Lizard*. University Press of Florida. (1988)

60 Domínguez-Rodrigo, M., de Juana, S., Galán A.B., Rodríguez, M. A new protocol to differentiate trampling marks from butchery cut marks. *Journal of Archaeological Science* 36: 2643-2654 (2009)

61 Fernandez-Jalvo, Y. & Andrews, P. *Atlas of Taphonomic Identifications* (Springer, 2016)

62 Behrensmeyer, A.K., Gordon, K.D., Yanagi, G.T. Trampling as a cause of bone surface damage and pseudo-cutmarks. *Nature* 319:768-771 (1986)

63 Shipman, P. Early hominid lifestyle hunting and gathering or foraging and scavenging? In J. Clutton-Brock and C. Girgson (eds) *Animal and archaeology, hunters and their prey*. *BAR International Series* 163: 31-49 (1983)

64 Crader, D.C., Recent single-carcass bone scatters and the problem of 'butchery' sites in the archaeological record. In J. Clutton-Brock and C. Girgson (eds) *Animal and archaeology, hunters and their prey*. *BAR International Series* 163: 107-141 (1983)

65 Inizan, M.-L., Reduron-Ballinger, M., Roche, H., Tixier, J. *Technology of the knapped stone*. CREP, Nanterre, 193p. (1999)

66 Simanjuntak, T, Sémah, F., Gaillard, C. The Palaeolithic in Indonesia: Nature and chronology. *Quaternary International* 223-224:418-421 (2010)

67 von Koenigswald, G.H.R. and Gosh, A.K. Stone implements from the Trinil beds of Sangiran, Central Java I and II. *Nederlandse Akademie, Proceedings Series B Physical Sciences* 76(1):1-34 (1973)

68 Falguères, C., Sémah, F., Saleki, H., Hameau, S., Tu, H., Féraud, G., Simanjuntak, H., Widianto, H. Geochronology of early human settlements in Java: What is at stake? *Quaternary International* 416:5-11 (2016)

69 Sémah, F., Sémah, A-M., Djubiantono, T., Simanjuntak, H.T. Did they also make stone tools? *Journal of Human Evolution* 23:439-446 (1992)

70 Simanjuntak, T. and Sémah, F. A new insight into the Sangiran flake industry. *Indo-Pacific Prehistory Association Bulletin* 14:22-26 (1996)

71 Moigne, A.M., Due Awe, R., Sémah, F., Sémah, A.M. The cervids from the Ngebung site (Kabuh series, Sangiran Dome, Central Java) and their biostratigraphical significance. *Modern Quaternary Research in Southeast Asia*, 18:31-44 (2004)

72 Sémah, F. La position stratigraphique du site de Ngebung 2 (dôme de Sangiran, Java Central, Indonésie). In F. Sémah, C. Falguères, D. Grimaud-Hervé & A-M. Sémah (eds) *Origine des peuplements et chronologie des cultures paléolithiques dans le Sud-Est asiatique*, Colloque International de la Fondation Singer Polignac, Paris, p.299-330 (2001)

73 Brumm, A., Jensen, G.M., van den Bergh, G.D., Morwood, M.J., Kurniawan, I., Aziz, F., Storey, M. Hominins on Flores, Indonesia, by one million years ago. *Nature* 464:748-753 (2010)

74 Brumm, A., van den Bergh, G.D., Storey, M, Kurniawan, I., Alloway, B.V., Satiawan, R., Setiyabudi, E., Grün, R., Moore, M.W., Yurnaldi, D., Puspaningrum, M.R., Wibowo, U.P., Insani, H., Sutisna, I., Westgate, J.A., Pearce, N.J.G., Duval, M., Meijer, H.J.M., Aziz, F., Sutikna, T., van der Kaars, S., Flude, S., Morwood, M.J. Age and context of the oldest known hominin fossils from Flores. *Nature* 534, 249-253 (2016)

75 Yamei, H., Potts, R., Baoyin, Y., Zhengtang, G., Deino, A., Wei, W., Clark, J., Guangmao, X., Weiwen, H. Mid-Pleistocene Acheulean-like stone technology of the Bose Basin, South China. *Science* 287:1622-1626 (2000)

76 Pawlik, A.F. and Ronquillo, W.P. The Palaeolithic in the Philippines. *Lithic technology* 28(2):79-93 (2003)

77 Pawlik, A.F. The Palaeolithic site of Arubo 1 in central Luzon, Philippines. *Indo-Pacific Prehistory Association Bulletin* 24:3-12 (2004)

78 Pawlik, A.F. Acheulean in Nueva Ecija? *Hukay* 4:1-22 (2002)

79 Dizon, E.Z. and Pawlik, A.F. The lower Palaeolithic record in the Philippines. *Quaternary International* 223-224:444-450 (2010)

80 Peterson, W. *Anomalous archaeological sites of Northern Luzon and models of Southeast Asian Prehistory*. Unpublished PhD Thesis. University of Hawaii, Honolulu, 248p. (1979)

81 Mijares, A.S.B., Détroit, F., Piper, P., Grün, R., Bellwood, P., Aubert, M., Champion, G., Cuevas, N., De Leon, A., Dizon, E. New evidence for a 67,000-year-old human presence at Callao Cave, Luzon, Philippines. *Journal of Human Evolution* 59, 123-132 (2010)

82 Moore, M.W., Sutikna, T., Jatmiko, Morwood, M.J., Brumm, A. Continuities in stone flaking technology at Liang Bua, Flores, Indonesia. *Journal of Human Evolution* 57:503-526 (2009)

83 Schick, K.D. and Toth, N.P. *Making silent stones speak: Human Evolution and the dawn of technology*. Simon and Schuster publishers. 351p. (1993)

84 Haynes, G. and Klimowicz, J. Recent elephant-carcass utilization as a basis for interpreting mammoth exploitation. *Quaternary International* 359-360:19-37.

85 Isaac, G. The Food-sharing behavior of Protohuman Hominids. *Scientific American* p.90-108 (1978)

86 Delagnes, A., Lenoble, A., Harmand, S., Brugal, J-P., Prat, S., Tiercelin, J-J., Roche, H. Interpreting pachyderm single carcass sites in the African Lower and Early Middle Pleistocene record: A multidisciplinary approach to the site of Nadung'a 4 (Kenya). *Journal of Anthropological Archaeology* 25:448-465 (2006)

87 Espigares, Ma. P., Martínez-Navarro, B., Palmqvist, P., Ros-Montoya, S., Toro, I., Agustí, J., Sala, R. *Homo* vs. *Pachycrocuta* : earliest evidence of competition for an elephant carcass between scavengers at Fuente Nueva 3 (Orce, Spain). *Quaternary International* 295:113-125

88 Radmilli, A.M., and Boschian, G. *Gli æscavi a Castel di Guido : il più antico giacimento di cacciatori del Paleolitico inferiore nell'Agro Romano*. Instituto italiano di preistoria e protostoria Firenze. 306p. (1996)

89 Anzidel, A.P., Bulgarelli, G.M., Catalano, P., Cerilli, E., Gallotti, R., Lemorini, C., Milli, S., Palombo, M.R., Pantano, W., Santucci, E. Ongoing research at the late Middle Pleistocene site of La Polledrara di Cecanibbio (central Italy), with emphasis on human-elephant relationships. *Quaternary International* 255:171-187 (2012)

90 Piperno, M. and Tagliacozzo, A. The elephant butchery area at the Middle Pleistocene site of Notarchirico (Venosa, Basilicata, Italy). In G. Cavarretta, P. Giota, M. Mussi & M.R. Palombo, *La Terra degli Elefanti - The World of Elephants International Congress*, Rome, p.230-236 (2001)

91 Wenban-Smith, F.F., Allen, P., Bates, M.R., Parfitt, S.A., Preece, R.C., Stewart, J.R., Turner, C., Whittaker, J.E. The Clactonian elephant butchery site at Southfleet Road, Ebbsfleet, UK. *Journal of Quaternary Science* 21(5):471-483 (2006)

92 Villa, P., Soto, E., Santonja, M., Pérez-González, A., Mora, R., Parcerisas, J., Sesé, C. New data from Ambrona: closing the hunting *versus* scavenging debate. *Quaternary International* 126-128:223-250 (2005)

93 Villa, P. Torralba and Aridos: elephant exploitation in Middle Pleistocene Spain. *Journal of Human Evolution* 19:299-309 (1990)

94 Mosquera, M., Saladié, P., Ollé, A., Cáceres, I., Huguet, R., Villalaín, J.J., Carrancho, A., Bourlès, D., Braucher, R., Vallverdú, J. Barranc de la Boella (Catalonia, Spain): an Acheulean elephant butchering site from the European late Early Pleistocene. *Journal of Quaternary Science* 30(7):651-666 (2015)

95 Aureli, D., Contardi, A., Giaccio, B., Jicha, B., Lemorini, C., Madonna, S., Magri, D., Marano, F., Milli, S., Modesti, V., Palombo, M.R., Rocca, R. *Palaeoloxodon* and Human interactions : depositional setting, chronology and archaeology at the Middle Pleistocene Ficoncella Site (Tarquinia, Italy). *PlosONE* 10(4): 1-27 (2015)

96 Gaudzinski, S., Turner, E., Anzidei, A.P., Àlvarez-Fernández, E., Arroyo-Cabrales, J., Cinq-Mars, J., Dobosi, V.T., Hannus, A., Johnson, E., Münzel, S.C., Scheer, A., Villa, P. The use of Proboscidean remains in every-day Palaeolithic life. *Quaternary International* 126-128 (2005)

97 De Vos, J., Sartono, S., Hardja-Sasmita, S., Sondar, P-Y. The fauna from Trinil, type locality of *Homo erectus* a reinterpretation. *Geologie en Mijnbouw* 61(2): 207-211 (1982)

98 Van den Bergh, G.D., Kaifu, Y., Kurniawan, I., Kono, R.T., Brumm, A., Stiyabudi, E., Aziz, F., Morwood, M.J. *Homo floresiensis*-like fossils from the early Middle Pleistocene of Flores. *Nature* 534: 245-248 (2016)

99 van den Bergh, G.D., de Vos, J., Sondaar, P.Y. 2001. The Late Quaternary palaeogeography of mammal evolution in the Indonesian Archipelago, Pal.Pal.Pal., 171: 385-408

100 Downing, Musser & Park 1998: “The first fossil record of small mammals from Sulawesi, Indonesia: the large murid Paruromys dominator, from the Late? Pliocene Walanae Formation”, in: Tomida, Y., Flynn, L.J., Jacobs, L.L. (eds), Advances in Vertebrate Paleontology and Geochronology. National Science Museum Monographs, 14, Tokyo)

101 Bahain, J.-J., Yokoyama, Y., Falguères, C., Sarcia, M.N. ESR dating of tooth enamel: a comparison with K-Ar dating. *Quaternary Science reviews* 11, 245-250 (1992)

102 Guérin, G., Mercier, N. Adamiec, G. Dose-rate conversion factors: update. *Ancient TL* 29:5–8 (2011)

103 Grün, R., Katzenberger-Apel, O. An alpha irradiator for ESR dating. *Ancient TL*, 12:35–38. (1994)

104 Brennan, B.J., Rink, W.J., McGuirl, E.L., Schwarcz, H.P., Prestwich, W.V. Beta doses in tooth enamel by ‘‘One Group’’ theory and the Rosy ESR dating software. *Radiation Measurements* 27:307–314 (1997)

105 Shao, Q., Bahain, J.-J., Dolo, J.-M., Falguères, C. Monte Carlo approach to calculate US-ESR ages and their uncertainties. *Quaternary Geochronology*, 22:99-106 (2014)